



Università
degli Studi
della Campania
Luigi Vanvitelli

**NEUTRINOLESS DOUBLE-BETA DECAY &
REALISTIC SHELL MODEL CALCULATIONS**

DOCTOR OF PHILOSOPHY THESIS

Settore scientifico-disciplinare FIS/04

CANDIDATE:

RICCARDO MANCINO

SUPERVISOR:

NUNZIO ITACO

Anni 2017-2021

Abstract

Neutrinoless double beta ($0\nu\beta\beta$) decay is an exceedingly rare and unique process that could reveal physics beyond the Standard Model and as such its search is currently amongst the major objectives of experimental physics. The observation of such decay could distinguish the fundamental nature of the neutrino, whether Dirac or Majorana, and determine the absolute scale of the neutrino masses.

The rate of this process depends on the nuclear matrix element ($M^{0\nu}$) associated with the transition and the fact that this can only be provided by theoretical calculations spurs the theoretical nuclear physics community to provide the most reliable calculations needed for the success of the experimental programs. It is in this way possible to discover or, at least, put an upper threshold to the value of the effective neutrino mass $\langle m_{\beta\beta} \rangle$.

In this work $M^{0\nu}$ has been calculated under the hypothesis of light-neutrino exchange for five nuclei of particular experimental interest: $^{48}\text{Ca} \rightarrow ^{48}\text{Ti}$, $^{76}\text{Ge} \rightarrow ^{76}\text{Se}$, $^{82}\text{Se} \rightarrow ^{82}\text{Kr}$, $^{130}\text{Te} \rightarrow ^{130}\text{Xe}$ and $^{136}\text{Xe} \rightarrow ^{136}\text{Ba}$.

The framework adopted to perform the calculation is the Realistic Shell Model (RSM) that offers a microscopic description of the nucleus starting from the bare nucleon-nucleon potential without resorting to empirical adjustments. As well as most of the cases these results are obtained within the limits of the closure approximation.

However, to better estimate the uncertainties associated with the closure approximation the nuclear matrix elements for ^{48}Ca and ^{136}Xe are calculated using both the closure approximation and a nonclosure method. Combining the two approaches in a mixed method with remarkable convergence properties allows to perform the calculations with a reasonable computational effort.

Contents

Introduction	3
1 Historical introduction	5
1.1 Double beta decay	6
1.2 Neutrinoless double β -decay	8
2 Dirac and Majorana neutrinos	10
2.1 Neutrino masses and mixing	10
2.2 Weyl representation	12
3 The Nuclear Matrix Element	16
3.1 The neutrinoless double-beta decay half-life	16
3.2 The NME	18
3.3 The closure approximation	20
3.4 Beyond the closure approximation	21
3.5 The partial matrix elements	22

4	The Realistic Shell Model	26
4.1	The nuclear shell model	26
4.2	The effective Hamiltonian	30
4.3	The Lee-Suzuki transformation	32
4.4	The Krenciglowa-Kuo iterative technique	37
4.5	The Lee-Suzuki iterative technique	38
4.6	The \hat{Q} -box vertex function	39
4.7	The effective operators	42
5	Results	47
5.1	Introduction	47
5.2	Spectroscopic properties	48
5.3	Nuclear matrix elements for double beta decay with two neutrinos	51
5.4	Nuclear matrix elements for neutrinoless double-beta decay within the closure approximation	54
5.5	Nuclear matrix elements for neutrinoless double-beta decay going beyond the closure approximation	66
6	Conclusions	75
	List of Figures	78
	List of Tables	80
	Bibliography	81

Introduction

Neutrinoless double beta ($0\nu\beta\beta$) decay is an exceedingly rare and unique process that could reveal physics beyond the Standard Model and as such its search is currently amongst the major objectives of experimental physics. The observation of such decay could distinguish the fundamental nature of the neutrino, whether Dirac or Majorana, and determine the absolute scale of the neutrino masses.

The rate of this process depends on the nuclear matrix element ($M^{0\nu}$) associated with the transition and the fact that this can only be provided by theoretical calculations spurs the theoretical nuclear physics community to provide the most reliable calculations needed for the success of the experimental programs. It is in this way possible to discover or, at least, put an upper threshold to the value of the effective neutrino mass $\langle m_{\beta\beta} \rangle$.

The aim of this thesis is the calculation of the neutrinoless double-beta decay nuclear matrix element for $^{48}\text{Ca} \rightarrow ^{48}\text{Ti}$, $^{76}\text{Ge} \rightarrow ^{76}\text{Se}$, $^{82}\text{Se} \rightarrow ^{82}\text{Kr}$, $^{130}\text{Te} \rightarrow ^{130}\text{Xe}$ and $^{136}\text{Xe} \rightarrow ^{136}\text{Ba}$ under the hypothesis of light-neutrino exchange.

The first chapter is dedicated to the introduction of the problem of neutrinoless double-beta decay as well as to provide a brief history of the contribution to the study of such phenomenon.

The second chapter explores the difference between Dirac and Majorana neutrino and how the possibility of neutrinoless double-beta decay can help distinguish the different mechanisms through which they acquire mass. Then it is shown the relation between these different mechanisms, the possible violation of the lepton number conservation and the occurrence of neutrino mixing. In recent years, this fields of research has seen several breakthroughs

and has emerged as one of the most active.

The third chapter is focused on the theory behind the actual calculation of the nuclear matrix element $M^{0\nu}$ and how it is connected to the relevant physical observable that is the half-life of the $0\nu\beta\beta$ decay. The different terms that make up the NME are shown as well as how to decompose the same in the total angular momentum \mathcal{J} of the neutron-neutron pair of the mother nucleus and in the total angular momentum J_k of the proton-neutron pair of the intermediate daughter nucleus.

In this chapter, also, it is introduced the closure approximation and how this approach has significant advantages in that it eliminates the computationally very taxing need of calculating a large number of intermediate daughter nuclei states. This approximation, however, introduces an intrinsic uncertainty and to have an estimate of that a method to go beyond the closure approximation is introduced. To cure the faults of both approaches it is also presented a method which combines both the non-closure and closure approaches.

In the fourth chapter of this thesis is provided an overview of the basic formalism of realistic shell-model calculations. More precisely, it is shown the derivation of the effective shell-model Hamiltonian and decay operators, starting from realistic nuclear potentials, within the framework of many-body perturbation theory. Some technical details are given intended to assist non-experts to follow the shell-model calculations included in this thesis.

The fifth chapter opens with a summary of the results obtained for the spectroscopic properties and double-beta decay with neutrinos of ^{48}Ca , ^{76}Ge , ^{82}Se , ^{130}Te and ^{136}Xe . These results are used as springboard to introduce and test the ones achieved for the neutrinoless double-beta decay nuclear matrix elements. The convergence properties and perturbative behaviour of the effective operator are examined. For ^{48}Ca and ^{136}Xe the results obtained going beyond the closure approximation are reported and particular attention is focused on the decomposition of the NME in terms of J_k .

The conclusion of this thesis is dedicated to examine the highlights of this work as well as to present its main perspectives.

Chapter 1

Historical introduction

In modern nuclear physics there is great interest in neutrino-less double beta ($0\nu\beta\beta$) decay. The discovery of the existence of this process could bring further understanding in the following fundamental aspects of particle physics:

1. lepton-number violation;
2. the presence of a neutrino mass and its nature;
3. the existence of right-handed currents in electroweak interactions.

All of these issues cannot be explained in the confines of the Standard Model (SM) of particle physics, therefore the detection of $0\nu\beta\beta$ decay would imply the discovery of new physics beyond the SM. This deduction is not an isolated one and is further reinforced by other experimental observations.

Interest in the neutrino sector of the SM has seen a significant peak in recent years after evidence for neutrino flavor oscillations was obtained from the results of atmospheric, solar and accelerator neutrino experiments.

Around the year 1972, the solar ν_e flux was first measured by R. Davis et al. in the Homestake experiment. It was found that the flux was smaller than the one predicted by the solar models. B. Pontecorvo suggested that this deficit of ν_e neutrinos could be explained with a mechanism similar to the

one of neutral kaon mixing [1, 2, 3]. This was taken as first indirect evidence for the existence of oscillations of neutrinos between different flavours.

In 2015 the Nobel Prize in Physics was assigned to Takaaki Kajita and Arthur B. McDonald for their key contributions to the experiments which demonstrated that neutrinos oscillate. More in detail, the experiment done at Sudbury Neutrino Observatory (SNO) by Arthur B. McDonald demonstrated that the ν_e from the Sun were in fact, reaching the Earth with a different "identity".

The Super-Kamiokande experiment lead by Takaaki Kajita, instead, made the discovery that atmospheric neutrinos switch between two identities ν_μ and ν_τ on their way from the atmosphere to the ground.

These results are proof that neutrinos have a non-zero mass rest, however, the experiments studying neutrino oscillations are not sensitive to the absolute scale of the neutrino masses, since they are only sensitive to the square of the difference of the masses Δm^2 . Moreover it is not possible to determine in an unambiguous way whether the mass term is a Dirac or Majorana.

The primary interest in the $0\nu\beta\beta$ decay process is that, if discovered, will automatically mean that the rest mass of at least one neutrino flavor is nonzero and is of Majorana origin.

1.1 Double beta decay

The theoretical possibility of double beta decay was studied practically immediately after the appearance of W. Pauli's neutrino hypothesis in 1930 and the development of β -decay theory by E. Fermi in 1933.

It was in 1935 that M. Goeppert-Mayer proposed for the first time the possibility of two neutrino double beta decay [4], a process in which there is a transformation of an (A, Z) nucleus to an $(A, Z+2)$ nucleus that is accompanied by the emission of two electrons and two anti-neutrinos.

$$(A, Z) \rightarrow (A, Z + 2) + 2e^- + 2\bar{\nu}_e \quad (1.1.1)$$

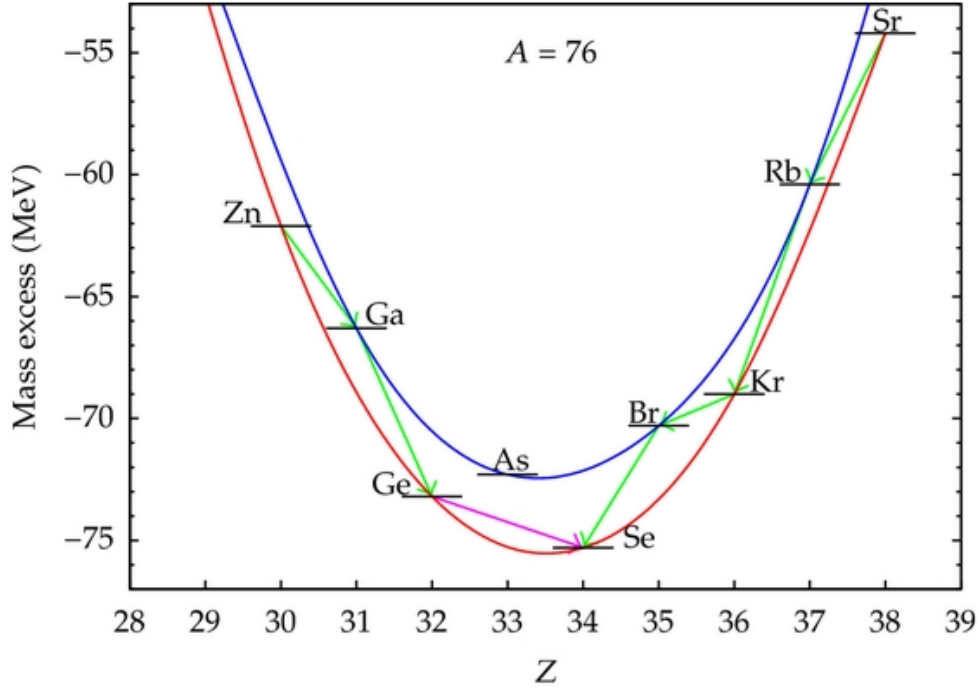


Figure 1: Isobar for nuclei with $A=76$. It is clear that, while the direct β -decay of ^{76}Ge in ^{76}As is not energetically allowed, ^{76}Se is a system at a lower energy and thus a possible end state for the double β -decay of ^{76}Ge .

To understand this phenomenon it is better to look at the isobars with even mass A as in Fig. 1. Usually a nucleus can undergo a beta decay if the energy of the final state is lower than the energy of the initial state. If this is not the case then the decay is energetically forbidden.

However, if the (A,Z) nucleus has a lower energy than the $(A, Z+1)$ one, but it is higher in energy than the $(A, Z+2)$ nucleus, then a double-beta decay is energetically admissible. Even if the emission of the electrons and the anti-neutrinos is simultaneous, it is possible to think of this as a two-step process where thanks to the Heisenberg uncertainty principle the system can violate the energy conservation principle for the time it takes to pass through the state $(A, Z+1)$. In this regard the process is simply a beta decay happening twice in rapid succession.

Such energetic considerations greatly limit the number of possible can-

didates for double beta decay. Until now only fourteen nuclei have been observed to undergo this process or its reverse, the double electron capture [5]. The experimental methods to measure the half-life of these nuclei vary from direct to geochemical and radiochemical.

$t_{1/2}(10^{21} \text{ yr})$	<i>ISOTOPE</i>	<i>TRANSITION</i>	<i>METHOD</i>	<i>DOCUMENT ID</i>	
• • • We do not use the following data for averages, fits, limits, etc. • • •					
> 0.87	^{134}Xe		EXO-200	1 ALBERT	17C
0.82 ±0.02 ±0.06	^{130}Te		CUORE-0	2 ALDUINO	17
0.00690±0.00015±0.00037	^{100}Mo		CUPID	3 ARMENGAUD	17
0.0274 ±0.0004 ±0.0018	^{116}Cd		NEMO-3	4 ARNOLD	17
0.064 +0.007 +0.012 -0.006 -0.009	^{48}Ca		NEMO-3	5 ARNOLD	16
0.00934±0.00022 +0.00062 -0.00060	^{150}Nd		NEMO-3	6 ARNOLD	16A
1.926 ±0.094	^{76}Ge		GERDA	7 AGOSTINI	15A
0.00693±0.00004	^{100}Mo		NEMO-3	8 ARNOLD	15
2.165 ±0.016 ±0.059	^{136}Xe		EXO-200	9 ALBERT	14
9.2 +5.5 ±1.3 -2.6	^{78}Kr		BAKSAN	10 GAVRILYAK	13
2.38 ±0.02 ±0.14	^{136}Xe		KamLAND-Zen	11 GANDO	12A
0.7 ±0.09 ±0.11	^{130}Te		NEMO-3	12 ARNOLD	11
0.0235 ±0.0014 ±0.0016	^{96}Zr		NEMO-3	13 ARGYRIADES	10
0.69 +0.10 ±0.07 -0.08	^{100}Mo	$0^+ \rightarrow 0_1^+$	Ge coinc.	14 BELLI	10
0.57 +0.13 ±0.08 -0.09	^{100}Mo	$0^+ \rightarrow 0_1^+$	NEMO-3	15 ARNOLD	07
0.096 ±0.003 ±0.010	^{82}Se		NEMO-3	16 ARNOLD	05A
0.029 +0.004 -0.003	^{116}Cd		$^{116}\text{CdWO}_4$ scint.	17 DANEVICH	03

Table 1: Half-life of the $2\nu\beta\beta$ decay in units of 10^{21} years from Ref. [5]. These data combined with the isotopic distribution and general availability of the candidates means that the focus of the future experiment on $0\nu\beta\beta$ decay is on ^{48}Ca ^{76}Ge , ^{82}Se , ^{130}Te and ^{136}Xe .

1.2 Neutrinoless double β -decay

E. Majorana in 1937 [6] demonstrated that theoretically the conclusions of the Fermi β -decay theory are left unchanged if one were to allow the existence of a particular type of neutrino which is its own antiparticle, that is if $\nu \equiv \bar{\nu}$. As such if the difference in energy between the (A, Z) and the $(A, Z+2)$

nuclei allow for the double beta decay with neutrinos it also must allow the double beta decay without neutrinos. Historically, G. Racah in 1937 and W. Furry in 1939 [7] introduced a scheme for the neutrinoless double beta decay through a virtual intermediate state.

$$(A, Z) \rightarrow (A, Z + 2) + 2e^- \quad (1.2.1)$$

In contrast to the double beta decay with the emission of two-neutrinos, neutrinoless double-beta decay has not yet been observed. Fig. 2 clearly show the difference between the two cases. While it is possible to "cut" the first diagram horizontally without interfering with the process the same operation is impossible to do so on the second diagram. The connection is provided by the exchange of Majorana neutrino ν_M . The synchronicity of the events also means that the exchanged neutrino is a virtual particle.

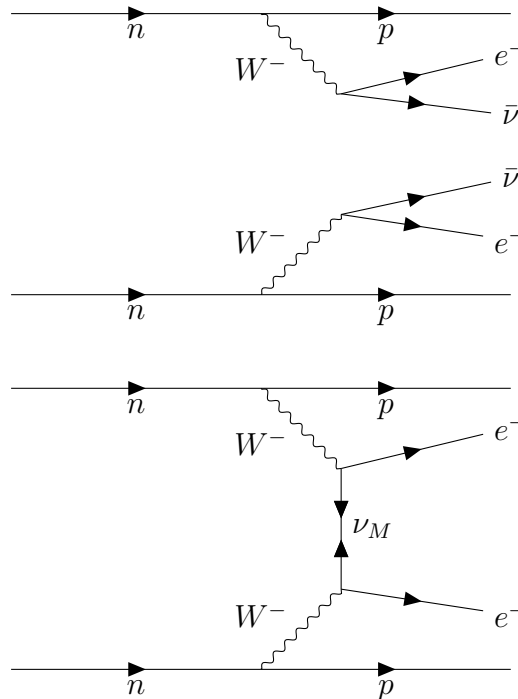


Figure 2: Double β -decay diagrams.

Chapter 2

Dirac and Majorana neutrinos

2.1 Neutrino masses and mixing

In this Chapter it is described the different mechanism through which between a Dirac or a Majorana fermion acquire mass. Then it is shown the relation between these different mechanisms with the possible violation of the lepton number conservation and with the phenomenon of neutrino oscillations. The occurrence of neutrino mixing follows naturally from the experimental evidence of massive neutrinos and its simplest form can be seen as a unitary transformation relating the flavor and mass eigenstates of neutrinos:

$$\begin{aligned} |\nu_\alpha\rangle &= \sum_i (U_{PMNS})_{\alpha i}^* |\nu_i\rangle \\ |\nu_i\rangle &= \sum_\alpha (U_{PMNS})_{\alpha i} |\nu_\alpha\rangle \end{aligned} \tag{2.1.1}$$

where $|\nu_\alpha\rangle$ is a neutrino state with definite flavor. $\alpha = e$ (electron), μ (muon) or τ (tauon), $|\nu_i\rangle$ is a neutrino state with definite mass m_i , $i = 1, 2, 3$. U_{PMNS} is the so called Pontecorvo-Maki-Nakagawa-Sakata neutrino mixing matrix.

In the case of the reference 3-neutrino mixing scheme the PMNS matrix is a 3×3 unitary matrix. It can be parametrised by 3 neutrino mixing angles and

in the case of Majorana neutrinos, by one Dirac and two Majorana physical CP violation (CPV) phases.

$$\begin{aligned}
U_{PMNS} &= \begin{pmatrix} U_{e1} & U_{e2} & U_{e3} \\ U_{\mu1} & U_{\mu2} & U_{\mu3} \\ U_{\tau1} & U_{\tau2} & U_{\tau3} \end{pmatrix} \\
&= \begin{pmatrix} c_{12}c_{13} & s_{12}c_{13} & s_{13}e^{-i\delta} \\ -s_{12}c_{23} - c_{12}s_{23}s_{13}e^{i\delta} & c_{12}c_{23} - s_{12}s_{23}s_{13}e^{i\delta} & s_{23}c_{13} \\ s_{12}s_{23} - c_{12}c_{23}s_{13}e^{i\delta} & -c_{12}s_{23} - s_{12}c_{23}s_{13}e^{i\delta} & c_{23}c_{13} \end{pmatrix} \times \\
&\times \begin{pmatrix} 1 & 0 & 0 \\ 0 & e^{i\alpha_1/2} & 0 \\ 0 & 0 & e^{i\alpha_2/2} \end{pmatrix}
\end{aligned} \tag{2.1.2}$$

where, $c_{ij} = \cos \theta_{ij}$ and $s_{ij} = \sin \theta_{ij}$, $0 \leq \theta_{ij} \leq \frac{\pi}{2}$, δ is the Dirac CPV phase and α_1 and α_2 are the two Majorana CPV phases.

The existing amount of data on neutrino oscillations can be explained within the 3-neutrino mixing scheme. However oscillation experiments can only provide us informations about the mass squared differences, the absolute values of neutrino masses m_1 , m_2 , and m_3 being currently unknown.

To proceed with the calculation of the decay rate for the $0\nu\beta\beta$ decay process it is then appropriate to define the so-called effective electron neutrino mass $\langle m_{\beta\beta} \rangle$

$$\langle m_{\beta\beta} \rangle = \left| \sum_i m_i U_{ei}^2 \right| \tag{2.1.3}$$

There is also the ambiguity on whether or not m_1 is heavier than m_3 . This is a consequence of the fact that the sign of Δm_{31}^2 cannot be determined from the existing data. This problem is known as the "neutrino mass hierarchy problem". If the mass of the neutrinos are arranged in crescent order, $m_1 < m_2 < m_3$, the hierarchy is called to "normal", while if it's not, that is, if $m_3 < m_1 < m_2$, the hierarchy is said to be "inverted".

<i>Parameter</i>	<i>BestFit</i> ($\pm\sigma$)	3σ
$\sin^2 \theta_{12}$	0.308 ± 0.017	$0.259 - 0.359$
$\sin^2 \theta_{23}$ (<i>NH</i>)	$0.437^{+0.033}_{-0.023}$	$0.374 - 0.628$
$\sin^2 \theta_{23}$ (<i>IH</i>)	$0.455^{+0.039}_{-0.031}$	$0.380 - 0.641$
$\sin^2 \theta_{13}$ (<i>NH</i>)	$0.0234^{+0.0020}_{-0.0019}$	$0.0176 - 0.0295$
$\sin^2 \theta_{13}$ (<i>IH</i>)	$0.0240^{+0.0019}_{-0.0022}$	$0.0178 - 0.0298$
$\Delta m_{\odot}^2 [10^{-5} eV^2]$	$7.54^{+0.26}_{-0.22}$	$6.99 - 8.18$
$\Delta m_A^2 [10^{-3} eV^2]$ (<i>NH</i>)	2.43 ± 0.06	$2.23 - 2.61$
$\Delta m_A^2 [10^{-3} eV^2]$ (<i>IH</i>)	2.38 ± 0.06	$2.19 - 2.56$

Table 2: Neutrino oscillation parameters from Ref. [8]

The mass hierarchy problem must be taken into account when examining the result of the experiments on $0\nu\beta\beta$ decay or when planning future ones.

2.2 Weyl representation

Fermions are elementary particles of the SM and spin $\frac{1}{2}$ representations of the Lorentz symmetry group. It is possible to derive a n -dimensional representation of the Lorentz algebra with the use of the following commutation relations

$$S^{\mu\nu} = \frac{i}{4}\{\gamma^\mu, \gamma^\nu\} \quad (2.2.1)$$

where the γ^μ are a set of $n \times n$ matrices satisfying the relations of the Dirac algebra

$$\{\gamma^\mu, \gamma^\nu\} = 2g^{\mu\nu} \times \mathcal{I}_{n \times n} \quad (2.2.2)$$

In the case of a four dimensional $n = 4$ Minkowski space and with the help of the Pauli sigma matrices σ^i we can achieve a 2×2 block representation of the Dirac γ^μ matrices

$$\gamma^0 = \begin{pmatrix} 0 & 1 \\ 1 & 0 \end{pmatrix}; \quad \gamma^i = \begin{pmatrix} 0 & \sigma^i \\ -\sigma^i & 0 \end{pmatrix} \quad (2.2.3)$$

This particular representation is called the Weyl representation, also called the chiral representation, and the generators of the Dirac algebra in this representation have the form

$$S^{0i} = -\frac{i}{2} \begin{pmatrix} \sigma^i & 0 \\ 0 & -\sigma^i \end{pmatrix}; \quad S^{ij} = \frac{e^{ijk}}{2} \begin{pmatrix} \sigma^k & 0 \\ 0 & \sigma^k \end{pmatrix} \quad (2.2.4)$$

Every fermion field Ψ that transform in agreement with these symmetries is called a Dirac spinor and respects the following Dirac equation

$$i\gamma^\mu \partial_\mu \Psi - m\Psi = 0 \quad (2.2.5)$$

However, to form a Lorentz scalar from two Dirac spinors its necessary to define the Dirac conjugate of the field as $\bar{\Psi} \equiv \Psi^\dagger \gamma^0$ which satisfies this complementary Dirac equation

$$-i\partial_\mu \bar{\Psi} \gamma^\mu - m\bar{\Psi} = 0 \quad (2.2.6)$$

The previous set of Dirac equations has some notable symmetries, one of which is the symmetry under charge conjugation $C = i\gamma^2\gamma^0$. The charge conjugation operator is a unitary operator which maps particle in antiparticle and its action can be expressed as

$$\begin{aligned} C : \Psi(x) &\rightarrow \Psi_C(x) \equiv C(\bar{\Psi}(x))^T, \\ C^{-1}\gamma_\mu C &= -\gamma_\mu^T. \end{aligned} \quad (2.2.7)$$

It is possible to add the condition that the antiparticle that obey the second Dirac equation coincides with the particle that obey the first Dirac equation unless a phase factor ξ

$$C(\bar{\Psi}(x))^T = \xi\Psi(x) \quad (2.2.8)$$

Such a fermion is called a Majorana fermion.

As is shown in Eq. 2.2.4 the generators of the Dirac algebra in the Weyl representation are in a clear block-diagonal form. It is then possible to reduce the 4-dimensional representation into two 2-dimensional representations.

$$\Psi = \begin{pmatrix} \Psi_L \\ \Psi_R \end{pmatrix} \quad (2.2.9)$$

The two-component fields Ψ_L and Ψ_R are thus called left-handed and right-handed Weyl spinors.

In the Lagrangian, the mass of a fermion field is the multiplicative factor in front of any bilinear invariant under the proper Lorentz transformations; it is possible to show that the only non-zero mass term has to be of the form $\bar{\Psi}_L\Psi_R$. This has profound implication in the way that a Dirac and a Majorana fermion can acquire mass.

If there are a left-handed field Ψ_{aL} and a right-handed field Ψ_{bR} that don't obey the Majorana condition $\Psi_{bR} \neq \xi_{ab}C\bar{\Psi}_{aL}^T$ for any a and b , the Dirac mass term of the Lagrangian has the form

$$\mathcal{L}_D = -\bar{\Psi}_{aL}(M_D)_{ab}\Psi_{bR} + h.c., \quad (2.2.10)$$

The Dirac mass matrix M_D is a $n \times n$ complex matrix and can be diagonalized by means of a bi-unitary transformation $M_D = U_L^\dagger M_D^d U_R$, leading to

$$\begin{aligned}\Phi_j &\equiv U_{Lja}\Psi_{aL} + U_{Rjb}\Psi_{bR}, \\ \mathcal{L}_D &= -\sum_j M_j \bar{\Phi}_j \Phi_j.\end{aligned}\tag{2.2.11}$$

Here Φ_j is a Dirac field having mass M_j .

Instead if the right-handed field needed to form a mass term obeys the Majorana condition $C\bar{\Psi}_{bL}^T \equiv \Psi_{bR}^C$, the mass term in the Lagrangian has the form:

$$\mathcal{L}_M = -\frac{1}{2}\bar{\Psi}_{aL}(M_M)_{ab}\Psi_{bR}^C + h.c.\tag{2.2.12}$$

and is called a Majorana mass term.

The Majorana mass matrix M_M is a complex symmetric matrix that can be diagonalized by means of a congruent transformation $M_M = U^\dagger M_M^d U^*$, leading to

$$\begin{aligned}\chi_j &\equiv U_{ja}\Psi_{aL} + U_{jb}^*\Psi_{bR}^C = C\bar{\Psi}_j^T \\ \mathcal{L}_D &= -\frac{1}{2}\sum_j M_j \bar{\chi}_j \chi_j\end{aligned}\tag{2.2.13}$$

Here χ_j is a Majorana field with mass M_j .

There is one major difference between the Dirac and Majorana mass terms. The Dirac mass term is invariant under the $U(1)$ transformations $\Psi_{aL} \rightarrow e^{i\alpha}\Psi_{aL}$, $\Psi_{bR} \rightarrow e^{i\alpha}\Psi_{bR}$ and thus conserves an additive quantum number. On the other side, the Majorana mass term in its most general form does not conserve any additive $U(1)$ charge possibly carried by the fields Ψ_{aL} .

This is the reason why the existence of Majorana neutrinos could mean the violation of the lepton number conservation. It's also worth noticing that a mixed Dirac and Majorana mass term Lagrangian can be cast in the form of a Majorana mass term and thus can be diagonalised as discussed above.

Chapter 3

The Nuclear Matrix Element

3.1 The neutrinoless double-beta decay half-life

In this thesis the calculation of the nuclear matrix element of the neutrinoless double β -decay process is undertaken in the hypothesis that the light-neutrino-exchange dominates the channel. As such the half-life of the $0\nu\beta\beta$ decay can be written as

$$\left[T_{1/2}^{0\nu}\right]^{-1} = G^{0\nu}|M^{0\nu}|^2\left(\frac{\langle m_{\beta\beta}\rangle}{m_e}\right)^2 \quad (3.1.1)$$

where $G^{0\nu}$ [9, 10, 11, 12, 13] is the so-called phase-space factor, which is obtained by integrating over the energies and angles of the final electrons and summing over the final states spins, $M^{0\nu}$ is the nuclear matrix element (NME), $\langle m_{\beta\beta}\rangle$ is the effective neutrino mass and m_e is the electron mass.

The effective neutrino mass is defined in terms of the neutrino mass eigenvalues m_i and the neutrino mixing matrix U_{ei}^2

$$\langle m_{\beta\beta}\rangle = \left|\sum_i m_i U_{ei}^2\right| \quad (3.1.2)$$

It is possible to rewrite Eq. 3.1.1 to express the neutrino effective mass in terms of $M^{0\nu}$, of the half-life $T_{1/2}^{0\nu}$ and of the so-called nuclear structure factor $F_N = G^{0\nu}|M^{0\nu}|^2$. In fact the aim of this work is to provide a reliable estimate of the value of the NME. Combining this with other constraints on the neutrino mixing parameters from current experiments, it is possible to estimate the half-life an experiment should measure in order to be sensitive to a particular value of the neutrino effective mass.

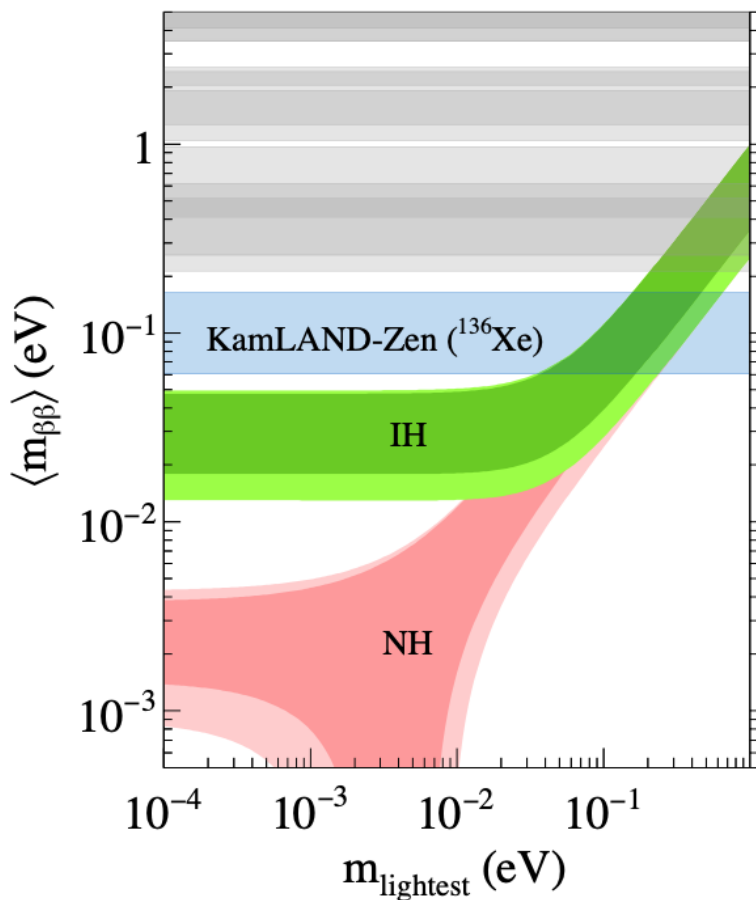


Figure 3: KamLAND-Zen limits on the effective Majorana neutrino mass $\langle m_{\beta\beta} \rangle$ from Ref. [14] as a function of the lightest neutrino mass m_{lightest} . The shaded regions are the predictions based on the values of neutrino oscillation parameters for the normal hierarchy (NH) and the inverted hierarchy (IH).

3.2 The NME

The Nuclear Matrix Element (NME) can be calculated as the sum of a Gamow-Teller (GT), a Fermi (F) and a Tensor (T) term

$$M^{0\nu} = M_{GT}^{0\nu} - \left(\frac{g_V}{g_A}\right)^2 M_F^{0\nu} + M_T^{0\nu} \quad (3.2.1)$$

where $g_V = 1$ is the vector coupling constant and $g_A = 1.2723$ is the axial coupling constant.

The nuclear matrix element is directly related to the transition between the wave functions of the parent $|i\rangle = |0_i^+\rangle$ and grand-daughter $|f\rangle = |0_f^+\rangle$ nuclei. This transition can be expanded as a sum over all the intermediate daughter $|k\rangle = |J_k^\pi\rangle$ states with a definite angular momentum J_k , parity π and energy E_k :

$$M_\alpha^{0\nu} = \sum_k \sum_{j_p j_{p'} j_n j_{n'}} \langle f | a_p^\dagger a_n | k \rangle \langle k | a_{p'}^\dagger a_{n'} | i \rangle \langle j_p j_{p'} | \tau_1^- \tau_2^- \Theta_\alpha^k | j_n j_{n'} \rangle \quad (3.2.2)$$

It is worth noting that the matrix elements in the previous expression are non antisymmetrized.

The operators Θ_α^k with $\alpha = \{GT, F, T\}$ contain the spin operators and the neutrino potential H_α , as well as the dependence on the energy of the intermediate daughter state E_k :

$$\begin{aligned} \Theta_{GT}^k &= \sigma_1 \cdot \sigma_2 H_{GT}^k(r) \\ \Theta_F^k &= H_F^k(r) \\ \Theta_T^k &= [3(\sigma_1 \cdot \hat{r})(\sigma_2 \cdot \hat{r}) - \sigma_1 \cdot \sigma_2] H_T^k(r) \end{aligned} \quad (3.2.3)$$

and

$$H_\alpha^k(r) = \frac{2R}{\pi} \int_0^\infty \frac{j_{n_\alpha}(qr)h_\alpha(q^2)q dq}{q + E_k - (E_i + E_f)/2} \quad (3.2.4)$$

where the value of the parameter $R = 1.2A^{1/3}fm$, the $j_{n_\alpha}(qr)$ are the spherical Bessel functions, $n_\alpha = 0$ for the Fermi and Gamow-Teller terms and $n_\alpha = 2$ for the Tensor term. The form functions $h_\alpha(q)$ for the light-neutrino exchange scenario are:

$$\begin{aligned} h_F(q^2) &= g_V^2(q^2) \\ h_{GT}(q^2) &= \frac{g_A^2(q^2)}{g_A^2} \left[1 - \frac{2}{3} \frac{q^2}{q^2 + m_\pi^2} + \frac{1}{3} \left(\frac{q^2}{q^2 + m_\pi^2} \right)^2 \right] + \\ &\quad + \frac{2}{3} \frac{g_M^2(q^2)}{g_A^2} \frac{q^2}{4m_p^2} \\ h_T(q^2) &= \frac{g_A^2(q^2)}{g_A^2} \left[\frac{2}{3} \frac{q^2}{q^2 + m_\pi^2} - \frac{1}{3} \left(\frac{q^2}{q^2 + m_\pi^2} \right)^2 \right] + \\ &\quad + \frac{1}{3} \frac{g_M^2(q^2)}{g_A^2} \frac{q^2}{4m_p^2} \end{aligned} \quad (3.2.5)$$

where the $g_{V,A,M}$ form factors can include nucleon finite size effects, which in the dipole approximation are given by:

$$\begin{aligned} g_V(q^2) &= \frac{g_V}{(1 + q^2/\Lambda_V^2)^2} \\ g_M(q^2) &= (\mu_p - \mu_n)g_V(q^2) \\ g_A(q^2) &= \frac{g_A}{(1 + q^2/\Lambda_A^2)^2} \end{aligned} \quad (3.2.6)$$

and it holds that $g_V = 1$, $g_A = 1.2723$, $(\mu_p - \mu_n) = 3.7$, $\Lambda_V = 850MeV$ and $\Lambda_A = 1086MeV$.

3.3 The closure approximation

Since the NME is expressed as a sum over all the possible intermediate daughter states there is a need to compute a very large number of states. This can be computationally taxing, especially for heavier nuclei.

However, it is possible to remove the energy dependence of the operator replacing the energy value in the denominator of the neutrino potential in Eq. 3.2.4. with its average constant value.

$$E_k - (E_i + E_f)/2 \rightarrow \langle E \rangle \quad (3.3.1)$$

In this way it is possible to introduce a new set of operators $\bar{\Theta}_\alpha \equiv \Theta_\alpha^k(\langle E \rangle)$ and to reduce the expression of the NME as:

$$\begin{aligned} M_\alpha^{0\nu} &= \sum_{j_p j_{p'} j_n j_{n'}} \langle j_p j_{p'} | \tau_1^- \tau_2^- \Theta_\alpha | j_n j_{n'} \rangle \sum_k \langle f | a_p^\dagger a_n | k \rangle \langle k | a_{p'}^\dagger a_{n'} | i \rangle \\ &= \sum_{j_p j_{p'} j_n j_{n'}} \langle j_p j_{p'} | \tau_1^- \tau_2^- \Theta_\alpha | j_n j_{n'} \rangle \langle f | a_p^\dagger a_{p'}^\dagger a_n a_{n'} | i \rangle \end{aligned} \quad (3.3.2)$$

The aforementioned substitution is called closure approximation since it exploits the completeness relation of the intermediate states. This approach has significant advantages because it eliminates the need of calculating a very large number of intermediate nuclei states, which could be computationally challenging, especially for heavy systems. One needs only to calculate the two-body transition densities between the parent and the grand-daughter nuclear states.

Obviously the issue related to this approach is to chose a value for this average energy, ideally one that should reproduce the exact value of the NME. This value of $\langle E \rangle$ can be estimated with the gross theory of β -decay and turns out to be of the order of 10 MeV [15, 16]. This results in a good approximation since the values of q that dominate the nuclear matrix elements are of the order of 100 - 200 MeV. This also mean that the nuclear

matrix elements are not very sensitive to the precise value of this average energy $\langle E \rangle$.

3.4 Beyond the closure approximation

In this section, it is presented a possible approach to go beyond the closure approximation so to evaluate its reliability. The only possible way to test the goodness of the approximation is to calculate the sum over k in Eq. 3.2.2 explicitly. This definitely present a challenge due to the large number of intermediate daughter states $|k\rangle$. In the simplest case of the ^{48}Ca in the fp shell model space the intermediate states are about 10^5 and as such it is extremely difficult to calculate and include all these states in the sum.

The nature of the neutrino potential as shown in Eq. 3.2.4, however, suggests that the higher in energy an intermediate state is the lower will be its contribution to the NME and therefore the difference between the closure and nonclosure calculations is concentrated mainly in the low-lying excitation energies. It is also reasonable to suppose that as a whole the overlap between the states, described in terms of the one body transition densities, will decrease with the increase of the excitation energy E_k of the intermediate states.

To test the convergence of the sum over k is it possible to introduce a cutoff state \bar{k} with an excitation energy \bar{E} and investigate the partial sum $M_\alpha^{0\nu}(\bar{E})$ all the intermediate states with $k < \bar{k}$

$$M_\alpha^{0\nu}(\bar{E}) = \sum_{k < \bar{k}} \sum_{j_p j_{p'} j_n j_{n'}} \langle f | a_p^\dagger a_n | k \rangle \langle k | a_{p'}^\dagger a_{n'} | i \rangle \langle j_p j_{p'} | \tau_1^- \tau_2^- \Theta_\alpha^k | j_n j_{n'} \rangle \quad (3.4.1)$$

To avoid double counting the contribution from these state it is appropriate to introduce the NME calculated with the operators $\bar{\Theta}_\alpha$.

$$\mathcal{M}_\alpha^{0\nu}(\bar{E}) = \sum_{k < \bar{k}} \sum_{j_p j_{p'} j_n j_{n'}} \langle f | a_p^\dagger a_n | k \rangle \langle k | a_{p'}^\dagger a_{n'} | i \rangle \langle j_p j_{p'} | \tau_1^- \tau_2^- \bar{\Theta}_\alpha | j_n j_{n'} \rangle \quad (3.4.2)$$

The difference between the previous Eq. 3.4.1 and 3.4.2 is the exact value difference between the closure and the non-closure approach when the excitation energy $E_k < \bar{E}$. It stands to reason that if the cut-off in the number of intermediate state were removed, i.e. for $\bar{E} \rightarrow \infty$, Eq. 3.4.2 would recover the result in closure approximation.

$$\mathcal{M}_\alpha^{0\nu}(\infty) = \sum_{j_p j_{p'} j_n j_{n'}} \langle f | a_p^\dagger a_n a_{p'}^\dagger a_{n'} | i \rangle \langle j_p j_{p'} | \tau_1^- \tau_2^- \bar{\Theta}_\alpha | j_n j_{n'} \rangle \quad (3.4.3)$$

To compensate for the shortcomings of both approaches it is possible to introduce a method which combines both the non-closure and closure approaches, by introducing a mixed NME that depends on the energy \bar{E} of the cut-off state \bar{k} .

$$\bar{M}_\alpha^{0\nu}(\bar{E}) = M_\alpha^{0\nu}(\bar{E}) - \mathcal{M}_\alpha^{0\nu}(\bar{E}) + \mathcal{M}_\alpha^{0\nu}(\infty) \quad (3.4.4)$$

It is reasonable to suppose that the convergence properties of the mixed NME $\bar{M}_\alpha^{0\nu}(\bar{E})$ are better than those of its single separate components. Since the difference $M_\alpha^{0\nu}(\bar{E})$ and $\mathcal{M}_\alpha^{0\nu}(\bar{E})$ is reduced at higher excitation energies the two terms should cancel each other out. This also means that the result of this mixed approach is even less dependent on the exact value of $\langle E \rangle$. It is also obvious from Eq. 3.4.4 that for the limit $\bar{E} \rightarrow \infty$ one would recover the result for the full non-closure approach. This mixed beyond closure approach has been first applied by Sen'kov and Horoi in a shell-model calculation of the NME for ^{48}Ca [17]. However, it is worth pointing out that this mixed approach can be fruitfully applied in whatever many-body approach employed to calculate the NME.

3.5 The partial matrix elements

To better understand how the structure properties of the states involved in $0\nu\beta\beta$ decay can affect the value of the NME it will be useful to introduce two different partial matrix elements based on angular momentum recoupling.

At first it is possible to introduce the expression for the partial NME that corresponds to a definite intermediate state k .

$$M_{\alpha k}^{0\nu} = \sum_{j_p j_{p'} j_n j_{n'}} \langle f | a_p^\dagger a_n | k \rangle \langle k | a_{p'}^\dagger a_{n'} | i \rangle \langle j_p j_{p'} | \tau_1^- \tau_2^- \Theta_\alpha^k | j_n j_{n'} \rangle \quad (3.5.1)$$

where it then holds that:

$$M_\alpha^{0\nu} = \sum_k M_{\alpha k}^{0\nu} \quad (3.5.2)$$

It is then possible to perform a sum over all intermediate states k with a certain spin J_k :

$$M_\alpha^{0\nu}(J_k) = \sum_{k, J_k = \text{fixed}} M_{\alpha k}^{0\nu} \quad \text{and} \quad M_\alpha^{0\nu} = \sum_{J_k} M_\alpha^{0\nu}(J_k) \quad (3.5.3)$$

On the other hand it is also possible to perform the corresponding sum over all intermediate states when the single-particle orbitals $|j_p\rangle$, $|j_{p'}\rangle$ and $|j_n\rangle$, $|j_{n'}\rangle$ in the two-body matrix elements $\langle j_p j_{p'} | \tau_1^- \tau_2^- \Theta_\alpha^k | j_n j_{n'} \rangle$ are coupled into total spin \mathcal{J} as

$$|j_p j_{p'}, \mathcal{J} M\rangle = \sum_{m_p m_{p'}} C_{j_p m_p j_{p'} m_{p'}}^{\mathcal{J} M} |j_p m_p\rangle |j_{p'} m_{p'}\rangle, \quad (3.5.4)$$

in such a way that

$$M_\alpha^{0\nu}(\mathcal{J}) = \sum_{k, \mathcal{J} = \text{fixed}} M_{\alpha k}^{0\nu} \quad \text{and} \quad M_\alpha^{0\nu} = \sum_{\mathcal{J}} M_\alpha^{0\nu}(\mathcal{J}) \quad (3.5.5)$$

It is worth noting that while the decomposition of the NME in terms of $M_\alpha^{0\nu}(\mathcal{J})$ is always possible, the decomposition in $M_\alpha^{0\nu}(J_k)$ can only be performed when going beyond the closure approximation. It is also remarkable that the coupling of the single particle orbitals in the initial and final states to

good angular momentum makes way for the use of reduced matrix elements $\langle j_p j_{p'}, \mathcal{J} || \tau_1^- \tau_2^- \Theta_\alpha^k || j_n j_{n'}, \mathcal{J} \rangle$.

These can be employed not only when going beyond the closure approach but also within the closure approximation. However, to use these reduced matrix elements without resorting to the closure approximation, the total angular momentum coupling must change from the coupling of the proton-proton and neutron-neutron pair to \mathcal{J} to the coupling of the two proton-neutron pairs to J_k . This can be done with the following transformation:

$$|j_p j_n(J_k) j_{p'} j_{n'}(J_k); 00\rangle = \sum_{\mathcal{J}} \widehat{J}_k \widehat{J}_k \widehat{\mathcal{J}} \widehat{\mathcal{J}} \begin{Bmatrix} j_p & j_{p'} & \mathcal{J} \\ j_n & j_{n'} & \mathcal{J} \\ J_k & J_k & 0 \end{Bmatrix} |j_p j_{p'}(\mathcal{J}) j_n j_{n'}(\mathcal{J}); 00\rangle \quad (3.5.6)$$

where for the sake of simplicity the following hat notation $\widehat{J} = \sqrt{2J+1}$ has been introduced.

Then, it is possible with straightforward calculations to rewrite the partial NME terms $M_{\alpha k}^{0\nu}$ from Eq. 3.5.1 with the use of the reduced matrix elements as:

$$M_{\alpha k}^{0\nu} = \sum_{j_p j_{p'} j_n j_{n'}} \widehat{J}_k \widehat{J}_k \widehat{\mathcal{J}} (-1)^{j_n + j_{p'} + J_k + \mathcal{J}} \begin{Bmatrix} j_p & j_n & J_k \\ j_{n'} & j_{p'} & \mathcal{J} \end{Bmatrix} \langle j_p j_{p'}, \mathcal{J} || \tau_1^- \tau_2^- \Theta_\alpha^k || j_n j_{n'}, \mathcal{J} \rangle \rho_{np}(J_k, i \rightarrow k) \rho_{n'p'}(J_k, k \rightarrow f) \quad (3.5.7)$$

where the one-body transition densities (OBTD) ρ_{np} and $\rho_{n'p'}$ were introduced. In the proton-neutron formalism these can be written as

$$\rho_{np}(J_k, i \rightarrow k) = \widehat{J}_k^{-1} \langle k || [\hat{c}_p^\dagger \otimes \tilde{c}_n]_{J_k} || i \rangle \quad (3.5.8)$$

$$\rho_{n'p'}(J_k, k \rightarrow f) = \widehat{J}_k^{-1} \langle f || [\hat{c}_{p'}^\dagger \otimes \tilde{c}_{n'}]_{J_k} || k \rangle \quad (3.5.9)$$

With this approach it is therefore possible to split the calculation of the NME in two decoupled parts. On one hand there is the problem of computing the reduced matrix element of the operator. On the other hand all the problems regarding the calculation of the the intermediate states $|k\rangle$ have been transformed into the calculation of the OBTD.

Now that the main focus of this work has been introduced, it is apparent that to calculate the NME one has to compute the nuclear wave-functions involved in the $0\nu\beta\beta$ decay. Hence the need to have a reliable and effective way to obtain these wave-function.

The shell model is the tool in nuclear structure physics that will be used. When the model space contains all physically relevant degrees of freedom and the residual interaction is well adjusted, the shell model describes nuclear low-energies spectra and transition probabilities with good accuracy. The expansion of the wave function in the harmonic oscillator base allows to analyse the structure of the states in terms of different configurations.

The purpose of the following chapter will be to revise the basic ideas behind the nuclear shell model. In particular it will be described how to construct a basis from single-particle solutions, how to solve the many-particle problem and how to construct the effective Hamiltonian and operators starting from a realistic nucleon-nucleon potential.

Chapter 4

The Realistic Shell Model

4.1 The nuclear shell model

The nuclear shell model (SM) is a well known and widely used framework for the computation of nuclear structure properties. The basic assumption of the SM is to consider the nucleus as composed by nucleons that move independently of each other inside a spherically symmetric mean field with an additional strong spin-orbit term. This mean field potential represents the average interaction with the other nucleons and is usually described by a harmonic oscillator or a Woods-Saxon potential. The nucleons are considered to be non-relativistic point-like particles and as such without any internal structure.

This framework produces single-particle states clustered in groups of orbits, called "shells", that are close in energy. This is in accord with experimental observation of nuclei with "magic numbers" of protons and/or neutrons, that is, nuclei that are more tightly bound than their neighbours. These energy levels are sufficiently separated from each other so that the nucleus can be regarded as an inert core, made up by shells filled up with neutrons and protons paired to angular momentum and parity $J = 0^+$, and a certain number of external nucleons, called "valence" nucleons.

The main result of this approach is that it reduces the complex nuclear

many-body problem to an effectively single-particle one where only a few valence nucleons move independently in a reduced model space composed only by a single major shell that rests above the inert core. Already it is possible to use this approximation to describe successfully various nuclear properties, such as the angular momentum and parity of the ground states in odd-mass nuclei.

Even so, it is clear that there is a "residual" part of the interaction between the valence nucleons which is not taken into account by the central potential. In order to account for the low-energy structure of nuclei with two or more nucleons in the valence shells one has to include explicitly the residual interaction. This produces a mixing between the different configurations and removes the degeneracy of states belonging to the same configuration.

As an example, it is possible to study the case of a simple nucleus as ^{18}O and to solve the Schrödinger equation for the A-nucleon system. This allows the introduction of the general formalism that is needed in the effective interaction theory. In this exposition it is assumed, for the sake of simplicity, that a two-body force is sufficient to describe the interaction between nucleons. It is possible, however, to extend the formalism to include three-body forces without any loss of generality.

$$H|\Psi_\nu\rangle = E_\nu|\Psi_\nu\rangle \quad (4.1.1)$$

with

$$H = H_0 + H_1 \quad (4.1.2)$$

where

$$H_0 = \sum_{i=1}^A \left(\frac{p_i^2}{2m} + U_i \right) \quad (4.1.3)$$

and

$$H_1 = \sum_{i<j}^A V_{ij}^{NN} - \sum_{i=1}^A U_i \quad (4.1.4)$$

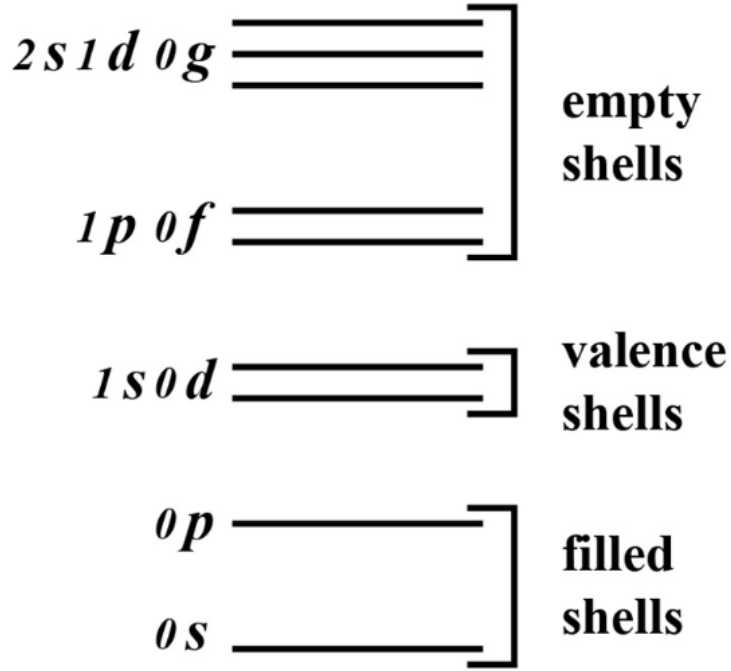


Figure 4: Energy shells that compose the core, valence space, and empty orbitals for ^{18}O .

V_{ij}^{NN} can be any of the nucleon-nucleon potentials that are readily available and that are able to reproduce with good accuracy all the known NN scattering data. The nuclear Hamiltonian has hence been broken up in the sum of two terms, a one-body term H_0 that accounts for the independent motions of the nucleons and a term H_1 for the residual interaction. It is possible to achieve this decomposition with the help of an auxiliary one-body potential U_i . The simplest and most frequently used choice for this auxiliary potential U is the three-dimensional harmonic oscillator potential.

$$U = \sum_{i=1}^A \frac{1}{2} m \omega^2 r_i^2 \quad (4.1.5)$$

The nucleus can be then thought of as a inert core, composed of a number of nucleons which fill a certain number of energy shells generated by the spectrum of the one-body Hamiltonian H_0 , plus a remainder of n interacting valence nucleons moving in the mean field H_0 . This is only possible thanks to the large energy gap between the shells that make so that one can disregard the remaining $A - n$ core nucleons, since they are frozen and completely fill the shells that are lowest in energy.

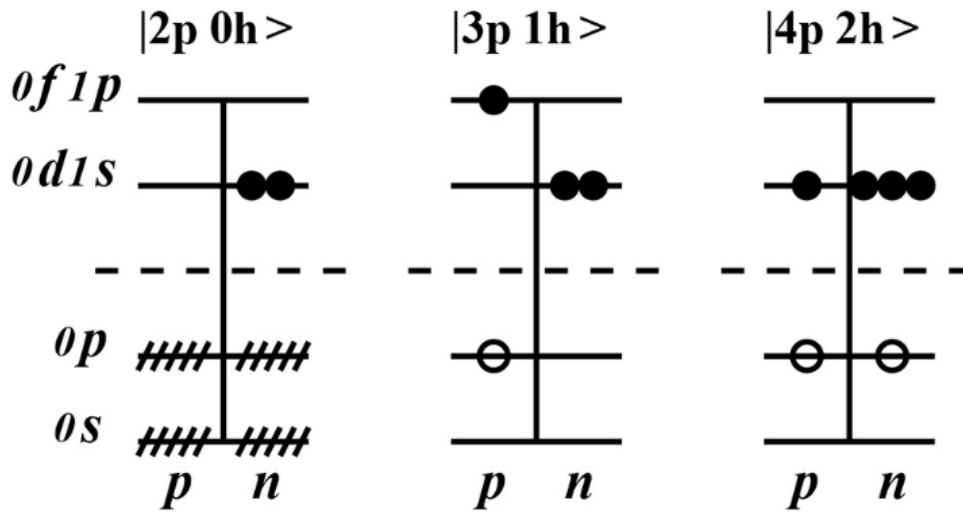


Figure 5: Some of the possible nucleon configurations for ^{18}O .

Since the closest magic number for a nucleus with $A = 18$ and $Z = 8$ is 8, it is reasonable to assume that the low energy states of ^{18}O will be dominated by configurations with a closed core of ^{16}O , that is with filled $0s_{1/2}$, $0p_{3/2}$ and $0p_{1/2}$ orbitals, and two neutrons in the valence shells $1s_{1/2}$, $0d_{5/2}$ and $0d_{3/2}$. As such, a suitable expression of the model space is in terms of the eigenvectors of the Hamiltonian H_0 .

$$|\Phi_i\rangle = \sum_{\alpha, \beta \in v.s.} C_{\alpha\beta}^i [a_{\alpha}^{\dagger} a_{\beta}^{\dagger}]_i |c\rangle, \quad i = 1, \dots, d, \quad (4.1.6)$$

where $|c\rangle$ represents the unperturbed core of the ^{16}O , that is obtained filling the $0s_{1/2}$, $0p_{3/2}$ and $0p_{1/2}$ orbits

$$|c\rangle = \prod_{\alpha \in f.s.} a_{\alpha}^{\dagger} |0\rangle, \quad (4.1.7)$$

and the index $i = 1, \dots, d$ represents all the other quantum numbers that are needed in order to determine the state, such as the total angular momentum.

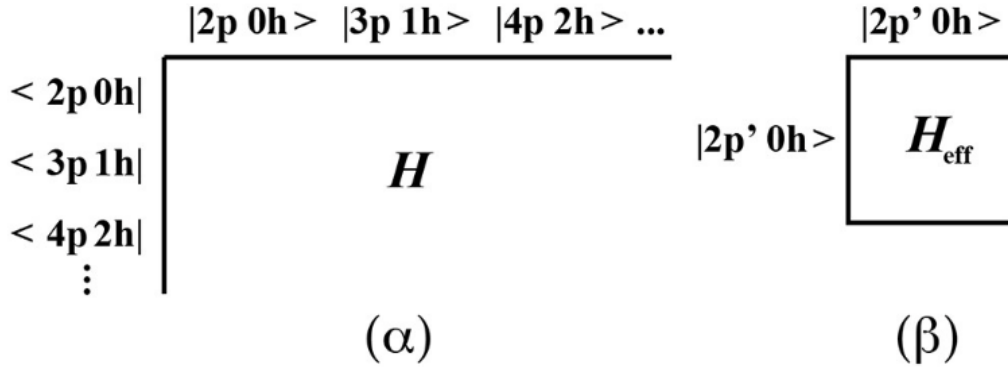


Figure 6: Representation of the matrices H and H_{eff} for ^{18}O .

However, this procedure does not account for any core excitation. It is always possible to introduce a particle-hole couple, as long as a particle exists in the core, and obtain a new configuration for ^{18}O as show in Fig. 5. In principle it is not possible to discard the contribution of these configurations. The solution of the full Schrödinger Equation 4.1.1 in the basis of these vectors, then, is tantamount to the diagonalization of the infinite-dimensional matrix H represented in Fig. 6.

4.2 The effective Hamiltonian

While it is not feasible to solve the problem in the complete Hilbert space it is possible to use approximate methods to solve this problem. One of the possible solutions is to reduce the eigenvalue problem of Eq. 4.1.1 to a model-space eigenvalue problem of a smaller matrix H_{eff} . This reduced Hilbert space can be expressed in terms of a finite subset of the eigenvectors of H_0 , as expressed in Eq. 4.1.6. The valence nucleons can then only have access to the major shell that is just above the closed core in energy.

The eigenvalues of the new Hamiltonian H_{eff} must belong to the set of eigenvalues of the previous Hamiltonian H . For this purpose one can define the projection operator P and its complement $Q = 1 - P$, which project respectively the complete Hilbert space onto the model space and onto its complementary space. These operators can be expressed in terms of the vectors in Eq. 4.1.6 as

$$P = \sum_{i=1}^d |\Phi_i\rangle\langle\Phi_i| \quad (4.2.1)$$

The operators P and Q are idempotent and decoupled, that is they satisfy the following properties:

$$\begin{aligned} P^2 &= P \\ Q^2 &= Q \\ PQ &= 0 \\ QP &= 0 \end{aligned} \quad (4.2.2)$$

The objective of the effective interaction theory is hence to reduce the full eigenvalue problem of Eq. 4.1.1 to a reduced model-space eigenvalue problem.

$$PH_{\text{eff}}P\Psi_\alpha = (E_\alpha - E_c)P\Psi_\alpha \quad (4.2.3)$$

where E_c is the ground-state energy of the core.

There are two main methods than one can take when tasked with the problem of deriving an effective Hamiltonian:

1. the phenomenological approach;
2. starting from the bare nuclear interactions and using an appropriate many-body theory.

Within the phenomenological approach, the effective hamiltonian contains some adjustable parameters that must be modified to reproduce a set of empirical data. Sometimes the two body-matrix elements themselves have been treated as free parameters. This framework has been very successful in describing a variety of nuclear structure phenomena.

On the other hand, starting from the bare interactions between nucleons, there are several ways to derive an effective SM Hamiltonian. Indeed, alongside the many well-established frameworks based on many-body perturbation theory or the Lee-Suzuki transformation, novel non-perturbative methods such as the no-core shell model (NCSM) with a core based on the Lee-Suzuki similarity transformation, the shell-model coupled cluster (SMCC), or the valence-space in-medium similarity renormalization group (VS-IMSRG), are presently employed.

All of these are non-perturbative methods that are rooted in many-body theory and provide different ways to obtain a H_{eff} . They share the same general theoretical approach, that is they obtain an expression for the effective Hamiltonian H_{eff} with the use of a similarity transformation acting on the original Hamiltonian H .

$$H_{\text{eff}} = e^{-\mathcal{G}} H e^{\mathcal{G}} \quad (4.2.4)$$

where the similarity transformation is obtained as the exponential of a generator \mathcal{G} that must obey the following decoupling condition:

$$QH_{\text{eff}}P = 0 \quad (4.2.5)$$

4.3 The Lee-Suzuki transformation

In this section it is displayed the formalism and the derivation of the effective SM Hamiltonian based on the similarity transformation introduced by Lee and Suzuki [18]. This method has been very successful since it makes possible a perturbative expansion of H_{eff} for open-shell systems outside a closed core.

As already reminded, the SM framework offers the possibility to decompose the nuclear Hamiltonian H as the sum of an unperturbed one-body mean-field term H_0 and the residual interaction Hamiltonian H_1 with the assistance of an auxiliary one-body potential U .

The significant energy gap between the shells allows us to regard the $A - n$ nucleons in the core as frozen. They completely fill the shells that are lowest in energy according to the spectrum of the one-body Hamiltonian H_0 . The remaining n interacting valence nucleons move in the mean field H_0 and occupy the SP states in the major shell situated (in energy) just above the closed core. The configurations allowed by the valence nucleons within this major shell define the model space, a reduced Hilbert space, onto which the new eigenvalue problem can be cast in the following form:

$$H_{\text{eff}}P|\Phi_i\rangle = E_\alpha P|\Phi_i\rangle, \quad i = 1, \dots, d, \quad (4.3.1)$$

The effective Hamiltonian H_{eff} is defined exclusively in the model space. This means that it is possible to define a more general Hamiltonian \mathcal{H} on the complete Hilbert space. This new Hamiltonian \mathcal{H} must have the same eigenvalue of the original Hamiltonian H of the A -nucleon system, but also, must satisfy the decoupling condition between the model space and the complement space, i.e. it must hold that

$$Q\mathcal{H}P = 0 \quad (4.3.2)$$

Within these conditions, the restriction of the Hamiltonian \mathcal{H} on the P space is the effective Hamiltonian H_{eff} that was looked for, that is:

$$H_{\text{eff}} = P\mathcal{H}P \quad (4.3.3)$$

The problem it is then to find an expression for the Hamiltonian \mathcal{H} in terms of the original Hamiltonian H . This can be obtained by way of a similarity transformation as it was in the case of Eq. 4.2.4, but this time defined in the complete Hilbert space.

$$\mathcal{H} = X^{-1}HX \quad (4.3.4)$$

A particularly useful choice of the generator of the transformation X is offered by Suzuki and Lee [18]. That is to consider an operator X defined as $X = e^\omega$. Is possible to take a ω that satisfies the following properties without any loss of generality:

$$\begin{aligned} \omega &= Q\omega P \\ P\omega P &= 0 \\ Q\omega Q &= 0 \\ P\omega Q &= 0 \end{aligned} \quad (4.3.5)$$

This also means that the operator ω is nilpotent, i.e. $\omega^2 = \omega^3 = \dots = 0$, and this leads to the following simple expression for the transformation:

$$X = 1 + \omega \quad (4.3.6)$$

In this way the effective hamiltonian H_{eff} and the decoupling condition from Eq. 4.2.5 can be written as:

$$H_{\text{eff}} = P\mathcal{H}P = PHP + PHQ\omega \quad (4.3.7)$$

The decoupling Eq. 4.3.7 on the whole Hilbert space can be solved and used to calculate the operator ω and rewritten as

$$QHP + QHQ\omega - \omega PHP - \omega PHQ\omega = 0 \quad (4.3.8)$$

The previous is a non-linear matrix equation that can be solved only if the hamiltonian H is explicitly known in the complete Hilbert space, however, this is not an easy task. This approach has been employed only for light nuclei within the *ab initio* framework and can be overly difficult for heavy nuclei with mass $A > 2$.

The standard method to overcome this obstacle is to introduce the vertex function \hat{Q} -box, which can be evaluated with the use of a perturbative expansion. For the sake of simplicity, in the following, the model space is assumed to be degenerate:

$$PH_0P = \epsilon_0P \quad (4.3.9)$$

Taking into account the previous consideration, the residual term of the effective Hamiltonian $H_1^{\text{eff}} = H_{\text{eff}} - PH_0P$ can be expressed with the help of the operator ω :

$$H_1^{\text{eff}} = P\mathcal{H}P - PH_0P = PH_1P + PH_1Q\omega \quad (4.3.10)$$

Recalling that the unperturbed hamiltonian H_0 is diagonal, it follows that the decoupling condition must be enforced only for residual interaction.

$$QHP = QH_0P + QH_1P = QH_1P \quad (4.3.11)$$

This fact can be used to rewrite Eq. 4.3.8 as:

$$\begin{aligned} QH_1P + QHQ\omega - \omega(PH_0P + PH_1P + PH_1Q\omega) &= \\ &= QH_1P + QHQ\omega - \omega(\epsilon_0P + H_1^{\text{eff}}) = 0 \end{aligned} \quad (4.3.12)$$

The previous equation can be used to obtain the following identity for the operator ω :

$$\omega = Q \frac{1}{\epsilon_0 - QHQ} QH_1P - Q \frac{1}{\epsilon_0 - QHQ} \omega H_1^{\text{eff}} \quad (4.3.13)$$

and with the help of Eq. 4.3.10 to write a recursive equation for the residual term of effective Hamiltonian $H_1^{\text{eff}}(\omega)$:

$$H_1^{\text{eff}}(\omega) = PH_1P + PH_1Q \frac{1}{\epsilon_0 - QHQ} - PH_1Q \frac{1}{\epsilon_0 - QHQ} \omega H_1^{\text{eff}} \quad (4.3.14)$$

It is helpful to introduce the definition the vertex function \hat{Q} -box:

$$\hat{Q}(\epsilon) = PH_1P + PH_1Q \frac{1}{\epsilon - QHQ} QH_1P \quad (4.3.15)$$

In this way the recursive equation in Eq. 4.3.14 can be rewritten as:

$$H_1^{\text{eff}}(\omega) = \hat{Q}(\epsilon_0) - PH_1Q \frac{1}{\epsilon_0 - QHQ} \omega H_1^{\text{eff}} \quad (4.3.16)$$

It is apparent from both of the Eq. 4.3.15 and 4.3.16 that configurations that are part of the complement space that have an energy close to the unperturbed energy of the configurations inside the model space may give rise to poles in the iterative solution of Eq. 4.3.16. These states are the so-called "intruder states" and this problem as pointed out by Schucan and Weidenmüller [19, 20] is therefore called "intruder-state problem".

There are many possible iterative techniques to solve the previous equation that are based on the calculation of the derivatives of the \hat{Q} -box. The two methods most commonly used are the Krenciglowa-Kuo (KK) [21] and the Lee-Suzuki (LS) [22, 18, 23].

It is worth noting that the KK and LS techniques do not necessarily provide the same effective hamiltonian and both require an unperturbed hamiltonian whose eigenstates which belong to the model space are degenerate. This is a direct consequence of the dependance on the energy of \hat{Q} -box. However, there are approaches that extends the validity of the standard KK and LS procedures for non degenerate spaces.

4.4 The Krenciglowa-Kuo iterative technique

The Krenciglowa-Kuo (KK) iterative technique is a procedure that can be used to solve the recursive equation 4.3.16. This approach is founded on the coupling of Eq. 4.3.13 and 4.3.16 that yields the following iterative equation for the effective Hamiltonian:

$$H_1^{\text{eff}}(\omega_n) = \sum_{m=0}^{\infty} \left[-PH_1Q \left(\frac{-1}{\epsilon_0 - QHQ} \right)^{m+1} QH_1P \right] [H_1^{\text{eff}}(\omega_{n-1})]^m \quad (4.4.1)$$

It is possible to highlight that the term that is inside the first set of square brackets of the previous equation is a quantity proportional to the m th derivative of the \hat{Q} -box calculated at $\epsilon = \epsilon_0$:

$$\hat{Q}_m(\epsilon_0) = -PH_1Q \left(\frac{-1}{\epsilon_0 - QHQ} \right)^{m+1} QH_1P = \frac{1}{m!} \left[\frac{d^m \hat{Q}(\epsilon)}{d\epsilon^m} \right]_{\epsilon=\epsilon_0} \quad (4.4.2)$$

In this way the Eq. 4.4.1 can be rewritten as

$$H_1^{\text{eff}}(\omega_n) = \sum_{m=0}^{\infty} \frac{1}{m!} \left[\frac{d^m \hat{Q}(\epsilon)}{d\epsilon^m} \right]_{\epsilon=\epsilon_0} [H_1^{\text{eff}}(\omega_{n-1})]^m = \sum_{m=0}^{\infty} \hat{Q}_m(\epsilon_0) [H_1^{\text{eff}}(\omega_{n-1})]^m \quad (4.4.3)$$

The effective Hamiltonian can then be written in terms of the \hat{Q} -box and its derivatives assuming as first step of the iteration that $H_1^{\text{eff}}(\omega_0) = \hat{Q}_m(\epsilon_0)$.

$$H^{\text{eff}} = \sum_{i=0}^{\infty} F_i \quad (4.4.4)$$

where the F_n terms are defined as:

$$\begin{aligned}
F_0 &= \hat{Q}(\epsilon_0) \\
F_1 &= \hat{Q}_1(\epsilon_0)\hat{Q}(\epsilon_0) \\
F_2 &= [\hat{Q}_2(\epsilon_0)\hat{Q}(\epsilon_0) + \hat{Q}_1(\epsilon_0)\hat{Q}_1(\epsilon_0)]\hat{Q}(\epsilon_0)
\end{aligned} \tag{4.4.5}$$

4.5 The Lee-Suzuki iterative technique

The Lee-Suzuki (Ls) iterative technique is an other approach that can be used to solve the recursive equation. This procedure is based on the rearranging of Eq. 4.3.16 with the help of the operators ω and \hat{Q} to single out an expression for the effective residual Hamiltonian:

$$H_1^{\text{eff}}(\omega) = \left(1 + PH_1Q \frac{-1}{\epsilon_0 - QHQ} QH_1P\omega\right)^{-1} \hat{Q}(\epsilon_0) \tag{4.5.1}$$

It is then straightforward to cast the previous equation in an iterative form based on the progression of the operators $\{\omega_n\}$.

$$H_1^{\text{eff}}(\omega_n) = \left(1 + PH_1Q \frac{-1}{\epsilon_0 - QHQ} QH_1P\omega_{n-1}\right)^{-1} \hat{Q}(\epsilon_0) \tag{4.5.2}$$

where, for the sake of clarity, the explicit expression of the operator ω_n is given by:

$$\omega_n = Q \frac{1}{\epsilon_0 - QHQ} QH_1P - Q \frac{1}{\epsilon_0 - QHQ} \omega_{n-1} H_1^{\text{eff}} \tag{4.5.3}$$

The usual approach solve the iteration is to impose the initial conditions by choosing $\omega_0 = 0$, so that the first terms of the series can be written as:

$$\begin{aligned}
H_1^{\text{eff}}(\omega_1) &= \hat{Q}(\epsilon_0) \\
\omega_1 &= Q \frac{1}{\epsilon_0 - QHQ} QH_1P
\end{aligned} \tag{4.5.4}$$

This, in turn, yields an expression for the operator \hat{Q} that will be used in the following steps of the iteration.

$$\hat{Q}_1(\epsilon_0) = -PH_1Q \frac{1}{\epsilon_0 - QHQ} Q \frac{1}{\epsilon_0 - QHQ} QH_1P = -PH_1Q \frac{1}{\epsilon_0 - QHQ} \omega_1 \quad (4.5.5)$$

The $n = 2$ terms of the series can be then written as:

$$H_1^{\text{eff}}(\omega_2) = \left(1 + PH_1Q \frac{-1}{\epsilon_0 - QHQ} QH_1P \omega_1 \right)^{-1} \hat{Q}_m(\epsilon_0) = \frac{1}{\hat{Q}_1(\epsilon_0)} \hat{Q}(\epsilon_0) \quad (4.5.6)$$

$$\omega_2 = Q \frac{1}{\epsilon_0 - QHQ} QH_1P - Q \frac{1}{\epsilon_0 - QHQ} \omega_1 H_1^{\text{eff}}(\omega_2) \quad (4.5.7)$$

It is therefore possible to extrapolate the general LS expression for the residual effective Hamiltonian H_1^{eff} :

$$H_1^{\text{eff}}(\omega_n) = \left[1 - \hat{Q}_1(\epsilon_0) \sum_{m=2}^{n-1} \hat{Q}_m(\epsilon_0) \prod_{k=n-m+1}^{n-1} H_1^{\text{eff}}(\omega_k) \right]^{-1} \hat{Q}(\epsilon_0) \quad (4.5.8)$$

4.6 The \hat{Q} -box vertex function

The techniques discussed previously are based on the calculation of the \hat{Q} -box function as defined in Eq. 4.3.15. To obtain a perturbative expansion of the \hat{Q} -box it is possible to expand the term $1/(\epsilon - QHQ)$ in the denominator as a power series

$$\frac{1}{\epsilon - QHQ} = \sum_{n=0}^{\infty} \frac{1}{\epsilon - QH_0Q} \left(\frac{QH_1Q}{\epsilon - QH_0Q} \right)^n \quad (4.6.1)$$

This in turn can be used to write the full perturbative expansion of the \hat{Q} -box function as follows:

$$\hat{Q}(\epsilon) = PH_1P + PH_1Q \sum_{n=0}^{\infty} \frac{1}{\epsilon - QH_0Q} \left(\frac{QH_1Q}{\epsilon - QH_0Q} \right)^n QH_1P \quad (4.6.2)$$

This perturbative expansion can be evaluated with the use of a diagrammatic procedure. The Goldstone diagrams take into account particle-hole excitations for the valence nucleons system and it is standard procedure for most perturbative derivations of the effective Hamiltonian H^{eff} is to include systems that have one and two valence nucleons. It is possible to include contributions from three-body diagrams when one has to consider more than two valence nucleons. As it is computationally highly demanding to perform calculations including higher-order sets of diagrams, SM Hamiltonians are derived accounting for \hat{Q} -box diagrams up to at most third order in perturbation theory.

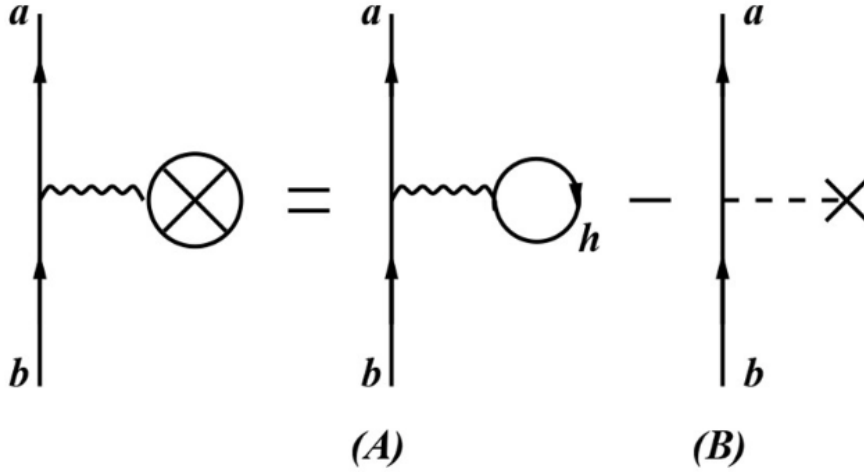


Figure 7: $(V - U)$ -insertion diagram: graph A minuend is the so-called self-energy diagram, while the graph B represents the matrix element of the harmonic oscillator potential $U = \frac{1}{2}m\omega^2r^2$.

As an example, in Fig. 7 it is shown the so called $(V - U)$ -insertion diagram. This particular diagram is composed of the self-energy diagram also called

the V-insertion diagram minus the auxiliary potential U-insertion. Its value is the expectation value of the effective residual interaction H_1^{eff} at first order in perturbation theory between any two SP states belonging to the model space.

The Goldstone expansion cannot be used in its bare form for nuclear calculations due to the strong short-range repulsion in the nucleon nucleon potential V_{NN} . This makes all the matrix elements far too large for this series to be meaningful. Therefore a resummation method has to be employed in order to take care of the strong short-range repulsion.

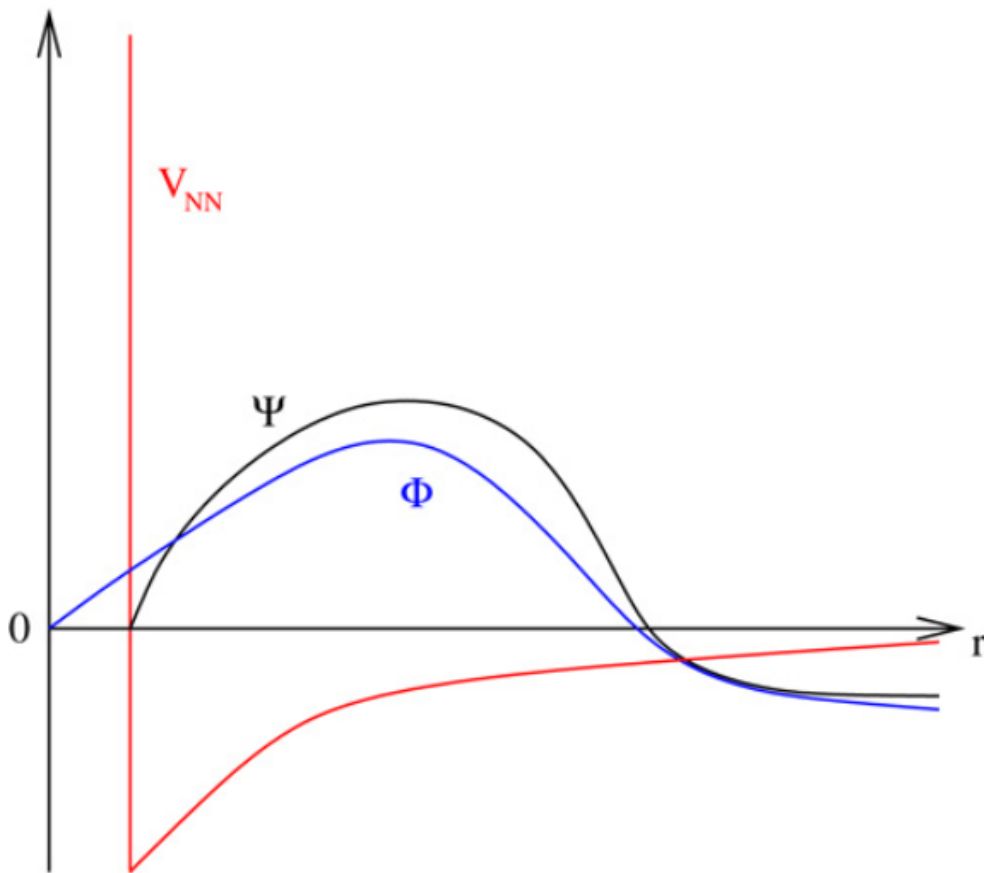


Figure 8: Radial dependence of the relative wave function Ψ of two nucleons interacting via a hard-core potential V_{NN} . Φ refers to the uncorrelated wave function.

There are different renormalisation procedures that can help to eliminate the short-range repulsive part of the NN interaction and thus can serve as a first step to the construction of the microscopic effective interaction. The traditional way is to calculate the so-called Brueckner reaction matrix [24] or G-matrix. This approach is based on the idea of treating exactly the interaction between a given pair of nucleons. The G matrix is then used to replace the NN interaction vertices once a rearrangement of the effective interaction perturbative series has been performed.

An other method to renormalize the NN interaction has been proposed [25, 26]. A low-momentum model space defined up to a cutoff momentum Λ is introduced and an effective potential V_{low-k} is derived from V_{NN} . This V_{low-k} satisfies a decoupling condition between the low and high-momentum spaces. Moreover, it is a smooth potential which preserves exactly the on-shell properties of the original potential and it is thus suitable to advantageously replace V_{NN} in realistic many-body calculations.

4.7 The effective operators

The energy of a state is but one of the physical observable of interest in nuclear physics. The effective SM offers a framework to find the matrix elements of operators that represent those physical observables such as wlecmagnetic transition rates, multipole moments and others.

It is reasonable to think that the eigenvectors $|\psi_\alpha\rangle = P|\Psi_\alpha\rangle$ obtained diagonalizing H^{eff} in the reduced model space are different from the solution of the full hamiltonian Ψ_α due to the fact that the degrees of freedom in the complement space Q are neglected. This, of course, influences the expectation value of any operator $\hat{\Theta}$ that act on the model space so that:

$$\langle\psi_\alpha|\hat{\Theta}|\psi_\beta\rangle \neq \langle\Psi_\alpha|\hat{\Theta}|\Psi_\beta\rangle \quad (4.7.1)$$

It is then apparent that one has to renormalize the operator $\hat{\Theta}$ defining an effective operator $\hat{\Theta}_{\text{eff}}$ such that its matrix element are unchanged.

$$\langle \psi_\alpha | \hat{\Theta}_{\text{eff}} | \psi_\beta \rangle = \langle \Psi_\alpha | \hat{\Theta} | \Psi_\beta \rangle \quad (4.7.2)$$

This $\hat{\Theta}_{\text{eff}}$ can be derived consistently within the many-body perturbation theory framework [25]. In particular, it is possible to have an expansion for the effective operator in terms of a $\hat{\Theta}$ -box function, which is the analogue of the \hat{Q} -box for the effective Hamiltonian H_{eff} . In the same spirit if one recalls from Eq. 4.3.7 that

$$H_{\text{eff}} = PH(P + \omega) \quad (4.7.3)$$

it is then possible to write the eigenvectors of the true Hamiltonian $|\Psi_\alpha\rangle$ and their orthonormal partners $\langle \tilde{\Psi}_\alpha|$ in terms of the eigenvectors of the effective Hamiltonian $|\psi_\alpha\rangle$.

$$\begin{aligned} |\Psi_\alpha\rangle &= (P + \omega)|\psi_\alpha\rangle \\ \langle \tilde{\Psi}_\alpha| &= \langle \tilde{\psi}_\alpha| (P + \omega^\dagger \omega) (P + \omega^\dagger) \end{aligned} \quad (4.7.4)$$

It is straightforward then to obtain the expression of the effective operator in the bra-ket for any general time-independent Hermitian operator Θ :

$$\Theta_{\text{eff}} = \sum_{\alpha\beta} |\psi_\alpha\rangle \langle \tilde{\Psi}_\alpha| \Theta | \Psi_\beta\rangle \langle \tilde{\psi}_\beta| \quad (4.7.5)$$

As is usually the case, if the eigenstates of the true Hamiltonian $|\Psi_\alpha\rangle$ are normalized such that $\langle \tilde{\Psi}_\alpha| = \langle \Psi_\alpha|$ then the following normalization condition must hold for the eigenstates of the effective Hamiltonian $|\psi_\alpha\rangle$:

$$\langle \tilde{\Psi}_\alpha| (P + \omega^\dagger \omega) | \Psi_\beta\rangle = 1 \quad (4.7.6)$$

Eq. 4.7.4 coupled with Eq. 4.7.5 can in turn be used to obtain the following operatorial equivalence between Θ_{eff} and Θ :

$$\Theta_{\text{eff}} = (P + \omega^\dagger \omega)^{-1} (P + \omega^\dagger) \Theta (P + \omega) \quad (4.7.7)$$

It is appropriate to introduce the explicit expression of the $\hat{\Theta}$ -box function in terms of the original operator Θ as:

$$\hat{\Theta} = (P + \omega^\dagger) \Theta (P + \omega) \quad (4.7.8)$$

In this way it is possible to obtain a simplified form for Eq. 4.7.7 as

$$\Theta_{\text{eff}} = (P + \omega^\dagger \omega)^{-1} \hat{\Theta} \quad (4.7.9)$$

In order to derive Θ_{eff} there are two tasks that must be completed. First one has to calculate the $\hat{\Theta}$ -box function, then the term $\omega^\dagger \omega$.

From the decoupling condition between the P and the Q spaces it is possible to write the $\hat{\Theta}$ -box function as the sum of different contribution:

$$\hat{\Theta} = \hat{\Theta}_{PP} + (\hat{\Theta}_{PQ} + h.c.) + \hat{\Theta}_{QQ} \quad (4.7.10)$$

where

$$\begin{aligned} \hat{\Theta}_{PP} &= P \Theta P \\ \hat{\Theta}_{PQ} &= P \Theta \omega P = \sum_{n=0}^{\infty} \hat{\Theta}_n (H_1^{\text{eff}})^n \\ \hat{\Theta}_{QQ} &= P \omega^\dagger \Theta \omega P = \sum_{n,m=0}^{\infty} (H_1^{\text{eff}})^m \hat{\Theta}_{nm} (H_1^{\text{eff}})^n \end{aligned} \quad (4.7.11)$$

Similarly to the derivatives of the \hat{Q} -box, the operators $\hat{\Theta}_m$ and $\hat{\Theta}_{mn}$ are defines as

$$\begin{aligned}
\hat{\Theta}_m &= \frac{1}{m!} \left. \frac{d^m \hat{\Theta}(\epsilon)}{d\epsilon^m} \right|_{\epsilon=\epsilon_0} \\
\hat{\Theta}_{mn} &= \frac{1}{m!n!} \left. \frac{d^m d^n \hat{\Theta}(\epsilon_1, \epsilon_2)}{d\epsilon_1^m d\epsilon_2^n} \right|_{\epsilon_1=\epsilon_0, \epsilon_2=\epsilon_0}
\end{aligned} \tag{4.7.12}$$

and with

$$\begin{aligned}
\hat{\Theta}(\epsilon) &= P\Theta P + P\Theta Q \frac{1}{\epsilon - QHQ} QH_1P \\
\hat{\Theta}(\epsilon_1, \epsilon_2) &= PH_1Q \frac{1}{\epsilon_1 - QHQ} Q\Theta Q \frac{1}{\epsilon_2 - QHQ} QH_1P
\end{aligned} \tag{4.7.13}$$

For the term $\omega^\dagger \omega$ it is possible to write ω in terms of the effective residual interaction H_1^{eff} as:

$$\omega = \sum_{n=0}^{\infty} (-1)^n \left(\frac{1}{\epsilon_0 - QHQ} \right)^{n+1} QH_1P (H_1^{\text{eff}})^n \tag{4.7.14}$$

It is then straightforward to obtain the following expression for the product $\omega^\dagger \omega$ recalling from Eq. 4.4.2 the definition of $\hat{Q}_m(\epsilon_0)$:

$$\omega^\dagger \omega = - \sum_{n=1}^{\infty} \sum_{m=1}^{\infty} ((H_1^{\text{eff}})^\dagger)^{n-1} \hat{Q}_{n+m-1}(\epsilon_0) (H_1^{\text{eff}})^{m-1} \tag{4.7.15}$$

The previous equation can be written entirely in terms of the \hat{Q} -box function and its derivatives as follows:

$$\omega^\dagger \omega = -\hat{Q}_1 + (\hat{Q}_2 \hat{Q} + h.c.) + (\hat{Q}_3 \hat{Q} \hat{Q} + h.c.) + (\hat{Q}_2 \hat{Q}_1 \hat{Q} + h.c.) + \dots \tag{4.7.16}$$

With the building blocks from Eq. 4.7.13 and Eq. 4.7.16, it is possible to write the perturbative expansion of a generic effective operator Θ^{eff} :

$$\Theta_{\text{eff}} = (P + \hat{Q}_1 + \hat{Q}_1 \hat{Q}_1 + \hat{Q}_2 \hat{Q}_2 + \hat{Q}_1 \hat{Q}_1 + \dots) \times (1 + \chi_0 + \chi_1 + \chi_2 + \dots) \quad (4.7.17)$$

where the χ_n terms are defined as

$$\begin{aligned} \chi_0 &= (\hat{\Theta}_0 + h.c.) + \hat{\Theta}_{00} \\ \chi_1 &= (\hat{\Theta}_1 \hat{Q} + h.c.) + (\hat{\Theta}_{01} \hat{Q} + h.c.) \\ \chi_2 &= (\hat{\Theta}_1 \hat{Q}_1 \hat{Q} + h.c.) + (\hat{\Theta}_2 \hat{Q} \hat{Q} + h.c.) (\hat{\Theta}_{02} \hat{Q} \hat{Q} + h.c.) + \hat{Q} \hat{\Theta}_{11} \hat{Q} \end{aligned} \quad (4.7.18)$$

It is also possible to write a more compact expression for the effective operator Θ_{eff} while keeping explicit the dependence of the effective operator on the effective Hamiltonian H_{eff} . This can be done by simply inserting the identity $\hat{Q} \hat{Q}^{-1} = 1$ in Eq. 4.7.17 to obtain

$$\Theta_{\text{eff}} = H_{\text{eff}} \hat{Q}^{-1} (\chi_0 + \chi_1 + \chi_2 + \dots) \quad (4.7.19)$$

This means that the χ_n series is truncated to a finite order and that the derivation of the perturbative expansions for $\hat{\Theta}$ is carried on consistently with the derivation of the \hat{Q} -box function.

Chapter 5

Results

5.1 Introduction

In the previous Chapter the basic theory of Realistic Shell Model was introduced and the framework for its application was established in a general context. It is time to apply the theory to the problem of the calculation of the nuclear matrix elements for neutrinoless double β -decay.

More precisely, in this Chapter they will be presented the SM results for the nuclei involved in the following decays: $^{48}\text{Ca} \rightarrow ^{48}\text{Ti}$, $^{76}\text{Ge} \rightarrow ^{76}\text{Se}$, $^{82}\text{Se} \rightarrow ^{82}\text{Kr}$, $^{130}\text{Te} \rightarrow ^{130}\text{Xe}$ and $^{136}\text{Xe} \rightarrow ^{136}\text{Ba}$.

The calculations for this work are based on the high-precision CD-Bonn NN potential [26]. To heal its non-perturbative behaviour induced by the repulsive high-momentum components, the so-called $V_{\text{low-k}}$ approach [27] has been employed. This provides a smooth potential which exactly preserves the on-shell properties of the original NN potential up to a chosen cutoff momentum Λ . As in other SM studies, the value of the cutoff has been chosen as $\Lambda = 2.6 \text{ fm}^{-1}$, since the role of the missing three-nucleon force (3NF) decreases as the $V_{\text{low-k}}$ cutoff is increased [28].

The choice of the model space has been tailored for the specific decay under investigation, and the corresponding effective Hamiltonian H_{eff} has

been derived in the framework of the Many-Body Perturbation Theory as described in previous chapter, including contribution from the \hat{Q} -box up to third order in perturbation theory. The details of the effective Hamiltonians can be found in Ref. [29].

The ^{48}Ca is, by far, the lightest nucleus and the easiest to compute of the group. The calculations adopt the valence space with the four proton and neutron single-particle orbitals $0f_{7/2}$, $1p_{3/2}$, $1p_{1/2}$ and $0f_{5/2}$ that are just above in energy of the double-magic core of ^{40}Ca .

Since within the pf model space there are no single particle states with unnatural parity, only states with positive parity can be constructed in this space. For these reasons, it is worth mentioning that ^{48}Ca , and sometimes lighter isotopes of Ca, are used as a paradigm for the double β -decay in shell-model calculations.

On the other hand, in the case of the medium mass ^{76}Ge and ^{82}Se the valence space consists of the four proton and neutron orbitals outside the double-magic core of ^{56}Ni . The relevant orbitals are $0f_{5/2}$, $1p_{3/2}$, $1p_{1/2}$, $0g_{9/2}$.

Lastly, the model space of ^{130}Te and ^{136}Xe encompasses the five proton and neutron orbitals outside the double-magic core of ^{100}Sn . The valence space is spanned by the neutron and proton orbitals $0g_{7/2}$, $1d_{5/2}$, $1d_{3/2}$, $2s_{1/2}$, $0h_{11/2}$ orbitals.

5.2 Spectroscopic properties

Figures 9, 10, 11, 12 and 13 show experimental [30, 31] and calculated low-energy spectra and $B(E2)$ strengths of parent and granddaughter nuclei involved in double- β decay of ^{48}Ca , ^{76}Ge , ^{82}Se , ^{130}Te and ^{136}Xe , respectively. As it can be seen, the RSM provides a satisfactory description of the low-lying excited states and the $B(E2)$ transition rates.

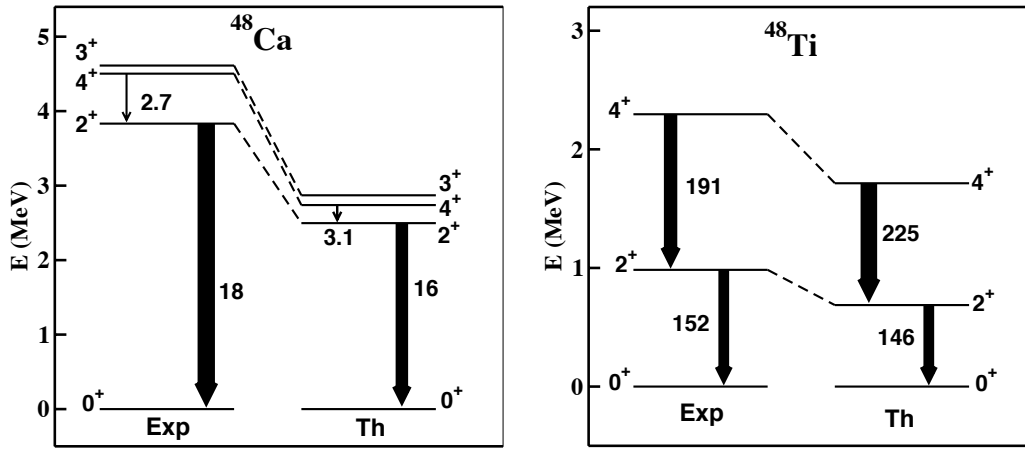


Figure 9: Spectroscopic properties, $B(E2)$ transition probabilities in e^2fm^4 for ^{48}Ca and ^{48}Ti . Fig. taken from Ref. [29].

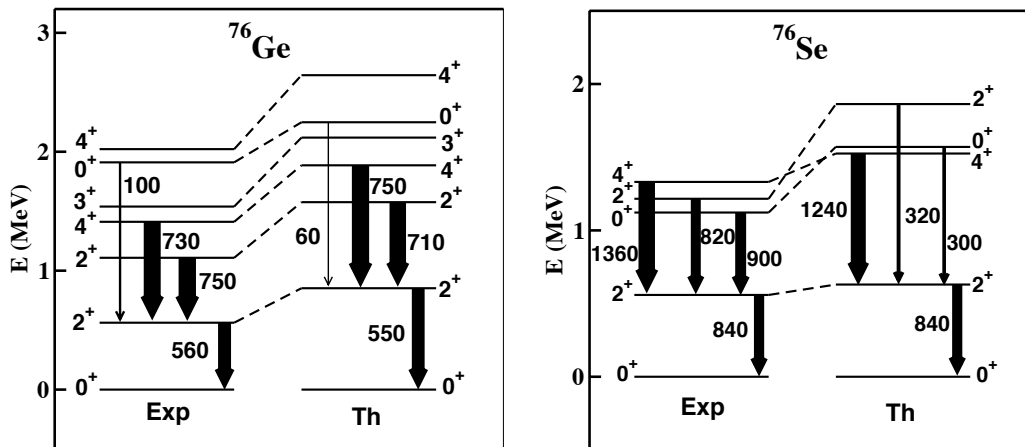


Figure 10: Spectroscopic properties, $B(E2)$ transition probabilities in e^2fm^4 for ^{76}Ge and ^{76}Se . Fig. taken from Ref. [29].

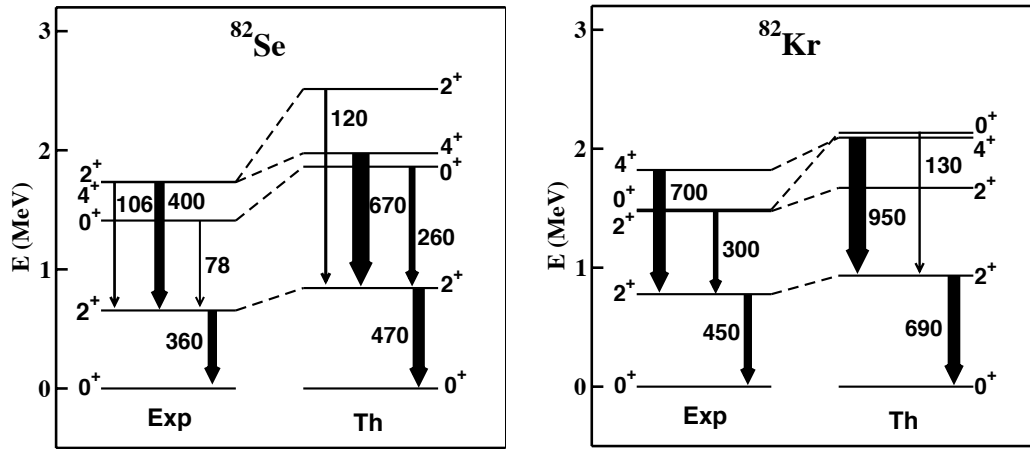


Figure 11: Spectroscopic properties, $B(E2)$ transition probabilities in e^2fm^4 for ^{82}Se and ^{82}Kr . Fig. taken from Ref. [29].

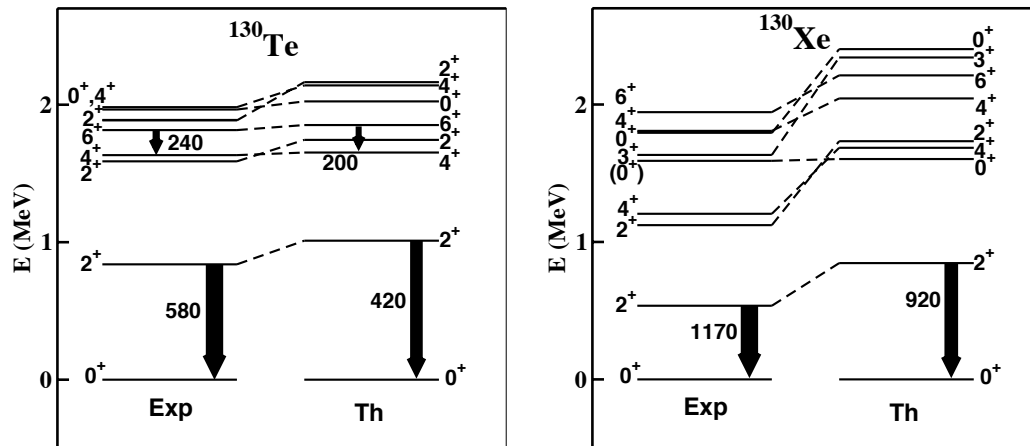


Figure 12: Spectroscopic properties, $B(E2)$ transition probabilities in e^2fm^4 for ^{130}Te and ^{130}Xe . Fig. taken from Ref. [29].

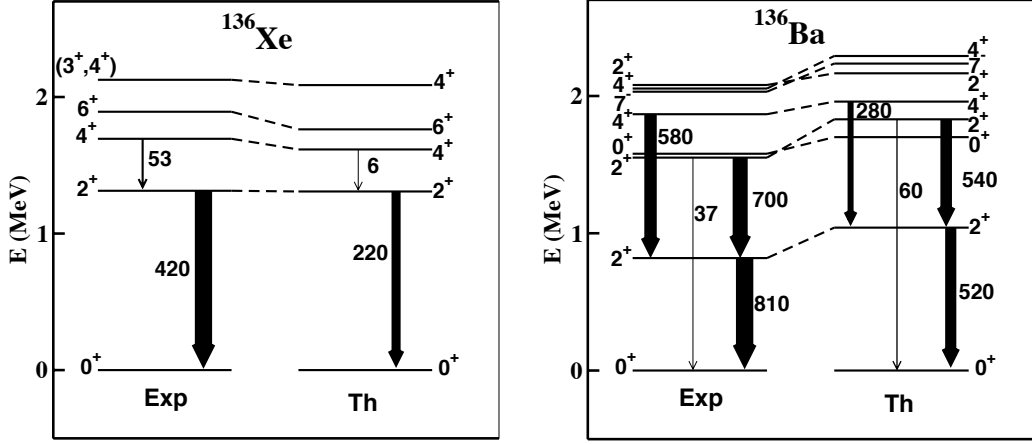


Figure 13: Spectroscopic properties, $B(E2)$ transition probabilities in $e^2 fm^4$ for ^{136}Xe and ^{136}Ba . Fig. taken from Ref. [29].

For sake of completeness, it is worth mentioning that in Ref. [29] they have been also calculated some $B(M1)$ strengths and magnetic dipole moments using an effective spin-dependent $M1$ operator, and their comparison with the available data turns out to be quite good.

5.3 Nuclear matrix elements for double beta decay with two neutrinos

In the present Section, the calculated NMEs of the $2\nu\beta\beta$ for ^{48}Ca , ^{76}Ge , ^{82}Se , ^{130}Te and ^{136}Xe are reported and compared with the available data. The $2\nu\beta\beta$ nuclear matrix element can be calculated through the expression:

$$M_{GT}^{2\nu} = \sum_k \frac{\langle 0_f^+ || \vec{\sigma}\tau^- || 1_k^+ \rangle \langle 1_k^+ || \vec{\sigma}\tau^- || 0_i^+ \rangle}{E_k - E_0} \quad (5.3.1)$$

where E_k is the excitation energy of the $J^\pi = 1_k^+$ intermediate state, and $E_0 = Q_{\beta\beta}(0^+)/2 + \Delta M$, with $Q_{\beta\beta}(0^+)$ and ΔM respectively the Q value of the transition and the mass difference of the initial and final nuclear states. The index k runs over all possible intermediate states induced by the given

transition operator. The theoretical values are compared with the experimental counterparts [32].

Decay	$M_{Th}^{2\nu}$	$M_{Ex}^{2\nu}$
$^{48}\text{Ca} \rightarrow ^{48}\text{Ti}$	0.026	0.035 ± 0.003
$^{76}\text{Ge} \rightarrow ^{76}\text{Se}$	0.104	0.106 ± 0.004
$^{82}\text{Se} \rightarrow ^{82}\text{Kr}$	0.109	0.085 ± 0.001
$^{130}\text{Te} \rightarrow ^{130}\text{Xe}$	0.061	0.0293 ± 0.0009
$^{136}\text{Xe} \rightarrow ^{136}\text{Ba}$	0.034	0.0181 ± 0.0006

Table 3: $2\nu\beta\beta$ nuclear matrix element employing effective Hamiltonians and decay operators derived starting from the CD-Bonn realistic potential at third order in perturbation theory compared with experiment [32] (in MeV^{-1}).

These quantities were calculated using the method of the Lanczos strength function as in reference [33], including as many as intermediate states to obtain at least a four-digit accuracy. The calculations were performed with the ANTOINE shell model code [34, 35].

From the inspection of Table 3, it can be seen that the agreement between the calculated and the experimental values of the $2\nu\beta\beta$ NMEs is quite good. To understand the role played by the use of effective GT transitions operators, in Fig. 12 it is reported a kind of correlation plot between the calculated $2\nu\beta\beta$ decay NMEs and the corresponding experimental values. The red symbols correspond to the results obtained employing the bare GT operators, while the black ones indicate the results obtained with the effective operators.

It is noticeable from the figure that the calculated NMEs using the bare operators systematically overestimate the experimental values, except the one corresponding to ^{48}Ca . On the other hand, the black points, obtained using effective GT operators, regroup themselves close to the identity, thus providing a nice reproduction of the observed data. These results may also be discussed in terms of the quenching of the axial vector coupling g_A , induced by the renormalization of the GT operators.

As a matter of fact, it is well known that the observed β -decay rates, $M^{2\nu}$ and Gamow-Teller transition strengths are systematically smaller than theoretical predictions. This leads to the need of quenching the free value of the axial coupling constant $g_A = 1.2723$ via a quenching factor q , whose numerical value depends on the nuclear structure model, the dimensions of the reduced Hilbert space, and the mass of the nuclei under investigation [36]. This quenching traces back to both the subnucleonic structure of the nucleons [37, 38, 39, 40] and the nuclear many-body effects, the latter arising from shortfalls of the nuclear many-body approaches used to compute the wave functions involved in the decay transitions.

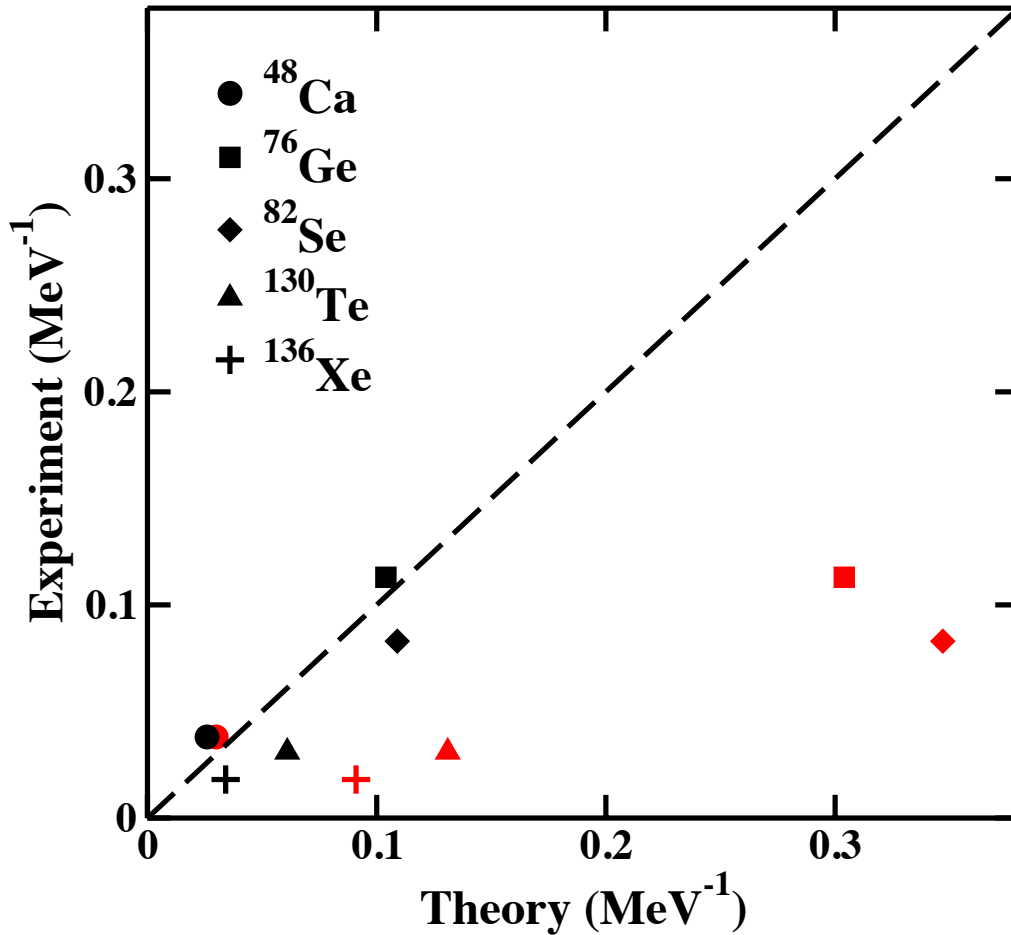


Figure 14: $2\nu\beta\beta$ nuclear matrix element (in MeV^{-1}). The red dots represent the result of the bare $M_{GT}^{2\nu}$ operator, while the black ones the effective $M_{GT}^{2\nu}$ operator at third order in perturbation theory. Fig. taken from Ref. [29]

5.4 Nuclear matrix elements for neutrinoless double-beta decay within the closure approximation

In this section are shown the RSM values of $M^{0\nu}$ calculated for ^{48}Ca , ^{76}Ge , ^{82}Se , ^{130}Te and ^{136}Xe . The $0\nu\beta\beta$ NMEs are obtained under the hypothesis that the mechanism that drives the decay is the light-neutrino exchange. Similarly to the case of the $2\nu\beta\beta$ NMEs, all SM ingredients are consistently derived from the high-precision CD-Bonn NN potential [26]. From this potential, within the framework of the RSM, a $V_{\text{low-k}}$ was obtained with a cut-off energy for $\Lambda = 2.6\text{fm}^{-1}$ [27]. This energy threshold ensures that the results are less affected by residual three-body force contributions and, consequently, by electroweak two-body current corrections.

The unperturbed Hamiltonian H_0 chosen for this work is the harmonic-oscillator (HO) one. The HO parameters of the unperturbed Hamiltonian are $\hbar\omega = 11, 10, 8$ MeV for model spaces placed respectively above ^{40}Ca , ^{56}Ni , and ^{100}Sn cores. These values were obtained according to the expression from Ref. [41] $\hbar\omega = 45A^{-1/3} - 25A^{-2/3}$ for $A = 40, 56$ and 100 .

As discussed previously, a H_{eff} has been calculated adopting the Many-Body perturbation theory. The \hat{Q} -box is expanded as a collection of one-body and two-body irreducible valence-linked Goldstone diagrams up to third order in the perturbation theory [42, 43].

All intermediate states whose unperturbed excitation energy is less than $E_{\text{max}} = N_{\text{max}}\hbar\omega$, with $N_{\text{max}} = 18$ have been taken into account. This value of N_{max} is chosen, as shown in Ref. [44], so to obtain convergence in SP energy spacings.

In Chapter 4 it has been described the derivation of an effective operator for a nuclear system with one or two valence nucleons. For example, in Fig. 15 all the two-body Θ_0 diagrams up to the second order are reported, the bare operator Θ being represented with a dashed line. Nevertheless the nuclei that are candidate to $0\nu\beta\beta$ decay are such that, within the SM, they are described in terms of a number of valence nucleons that is much larger

than 2.

For example, the double-beta decay of ^{48}Ca into ^{48}Ti involves 8 valence nucleons outside the doubly-magic ^{40}Ca . In such a case the expression of the effective operators should contain contribution up to a 8-body term. As the inclusion of all these contributions is unfeasible, just the leading terms of these many-body contributions in the perturbative expansion of the effective operator are included and reported in Fig. 16.

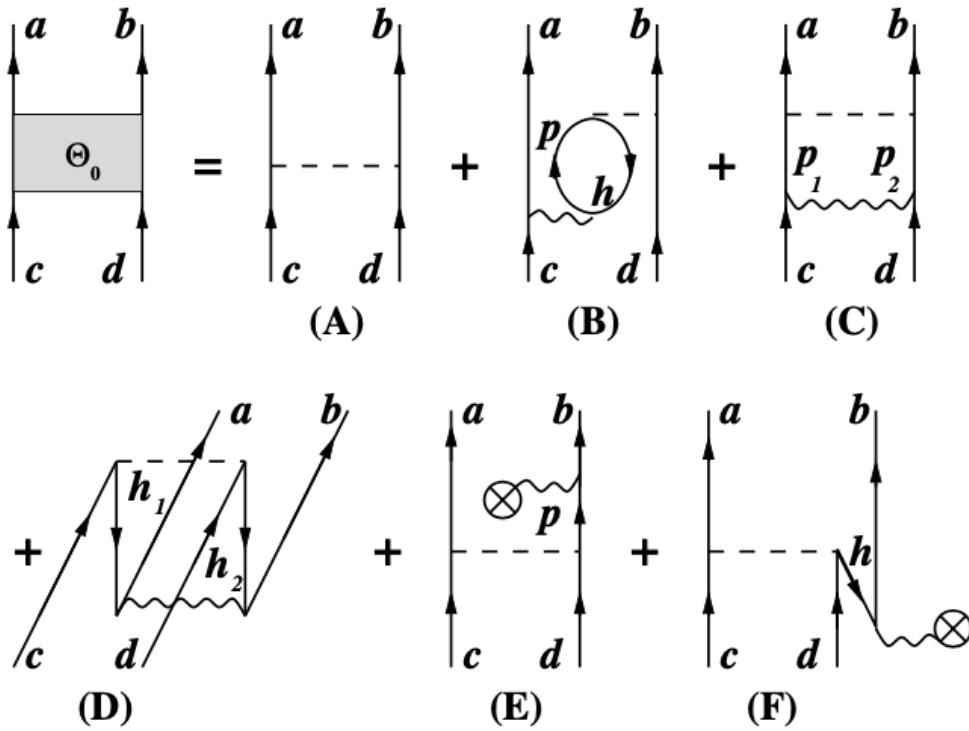


Figure 15: Second-order diagrams included in the perturbative expansion of $\hat{\Theta}$. The dashed lines indicate the bare operator Θ , the wavy lines the two-body potential $V_{\text{low}-k}$.

The two topologies of second order connected three valence nucleon diagrams (a) and (b) shown in Fig.16 correct the violation of the Pauli principle introduced by diagram (a') and (b') when one of the intermediate particle states is equal to m [45].

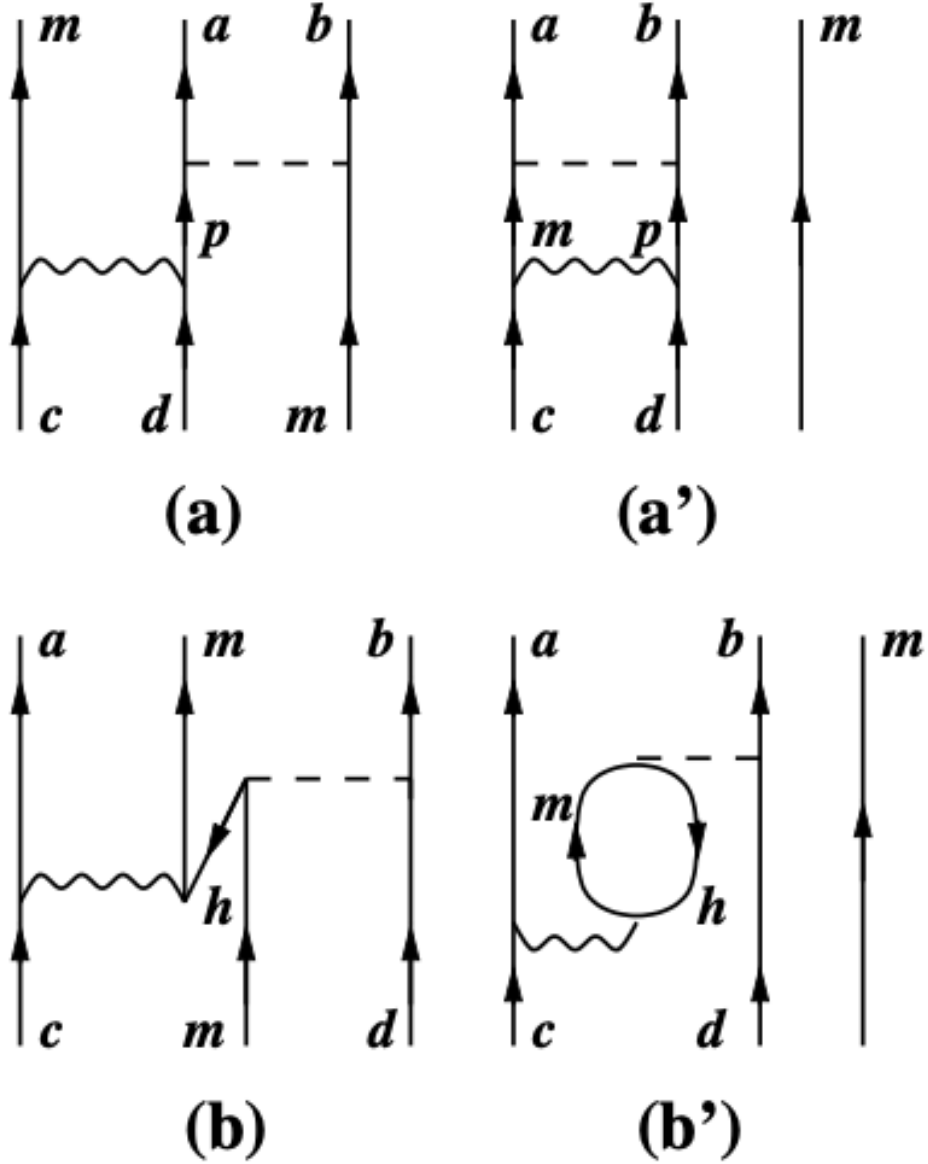


Figure 16: Second-order three-body diagrams which are included in the perturbative expansion of $\hat{\Theta}$. As in Fig. 15, the dashed line indicates the bare operator Θ , the $V_{\text{low-k}}$.

In this thesis the NMEs are calculated with the NATHAN SM code [46].

Since this code cannot manage three-body decay operators, an alternative method was employed. Summing over the partially filled model space orbitals, it is possible to recover a density-dependent two-body contribution at one-loop order from the three-body diagrams in Fig. 16. The same procedure has been performed to derive density-dependent two-body H_{eff} to study many-valence nucleon systems. Further details of this method can be found in Ref. [47, 48].

A well known issue when calculating the nuclear matrix element is how to include the contribution of the short-range correlations (SRC), arising from the fact that the action of the two-body $0\nu\beta\beta$ decay operator on an unperturbed (uncorrelated) wave function, as the one used in the perturbative expansion of Θ_{eff} , is not equal to the action of the same operator on the real (correlated) nuclear wave function.

The most common way to include SRC is by way of Jastrow type functions [49, 50], while in recent years SRC have been modeled by the so-called Unitary Correlation Operator Method (UCOM) [51, 52], this approach allowing to provide a unitary operator which prevents the overlap between the wave functions of a pair of nucleons [53].

In present calculations the inclusion of the SRC is treated with an original approach that is consistent with the $V_{\text{low-k}}$ procedure, and it has been introduced in Ref. [17]. To describe this approach is worth briefly recalling the main steps of the $V_{\text{low-k}}$ procedure.

The eigenvalue problem of the two-nucleon Hamiltonian $H^{NN}(k, k') = H_0(k, k') + V^{NN}(k, k')$, $H_0(k, k')$ being the kinetic-energy term, may be written in the full momentum space of the plane-waves basis $\langle k|\Psi_\nu\rangle$ in the following form:

$$\int_0^\infty [H_0(k, k') + V^{NN}(k, k')]\langle k|\Psi_\nu\rangle k^2 dk = E_\nu \langle k'|\Psi_\nu\rangle \quad (5.4.1)$$

The desired Hamiltonian $H_{\text{low-k}}(k, k') = H_0(k, k') + V_{\text{low-k}}(k, k')$ must be defined in a reduced subspace $P = \int_0^\Lambda |k\rangle\langle k| k^2 dk$, whose subset of eigenvalues $\{\tilde{E}_\mu\}_{\mu \in P}$ belongs to the set of eigenvalues $\{E_\nu\}$ of the Hamiltonian $H^{NN}(k, k')$ defined in full Hilbert space:

$$\int_0^\infty [H_0(k, k') + V_{\text{low-k}}(k, k')] \langle k | \Phi_\nu \rangle k^2 dk = \tilde{E}_\mu \langle k' | \Phi_\mu \rangle \quad (5.4.2)$$

This goal may be achieved through a similarity transformation $\Omega_{\text{low-k}}$, that leads to the identity $\mathcal{H} = \Omega_{\text{low-k}}^{-1} H^{NN} \Omega_{\text{low-k}}$. $\Omega_{\text{low-k}}$ needs to satisfy the decoupling condition which decouples the low-momentum subspace P from its complement $Q = 1 - P$:

$$Q\mathcal{H}P = Q\Omega_{\text{low-k}}^{-1} H^{NN} \Omega_{\text{low-k}} P = 0 \quad (5.4.3)$$

A very convenient expression of the operator $\Omega_{\text{low-k}}$ may be obtained according to the Lee-Suzuki formulation [18], which is:

$$\begin{aligned} \Omega_{\text{low-k}} P &= I_P & P \Omega_{\text{low-k}} &= 0 \\ Q \Omega_{\text{low-k}} P &= \omega & Q \Omega_{\text{low-k}} Q &= I_Q \end{aligned} \quad (5.4.4)$$

were I_P , I_Q represents the identity operator in the P and Q spaces, respectively. This form leads to a non-linear matrix equation for the ω operator, which can be solved using iterative techniques [54]:

$$QH^{NN}P + QH^{NN}Q\omega - \omega PH^{NN}P - \omega PH^{NN}Q\omega = 0 \quad (5.4.5)$$

Once Eq. 5.4.5 is solved and the operator ω is obtained, an hermitization procedure, based on the Cholesky decomposition of the operator $\Omega_{\text{low-k}}$ [54], evolves the Lee-Suzuki similarity transformation to a unitary transformation. The $V_{\text{low-k}}$, which is explicitly zero for momenta above the cutoff Λ , may now be suitable as an input for the derivation of H_{eff} by way of the many-body perturbation theory [43].

At this point, it is possible to take into account SRC first by calculating the $0\nu\beta\beta$ operator Θ within the momentum space and then by renormalizing it by means of $\Omega_{\text{low-k}}$ in order to consider effectively the high-momentum (short range) components of the NN potential, in a framework where their direct contribution is dumped by the introduction of a cutoff Λ .

Consequently, the Θ vertices appearing in the perturbative expansion of the $\hat{\Theta}$ box are substituted by the ones of the $\Theta_{\text{low-}k}$ operator, that is defined as $\Theta_{\text{low-}k} \equiv P\Omega_{\text{low-}k}\Theta\Omega_{\text{low-}k}^{-1}P$ for relative momenta $k < \Lambda$, and is equal to zero for $k > \Lambda$. It has been found that the effect in magnitude of this renormalization procedure is similar to the SRC modeled by the so-called Unitary Correlation Operator Method (UCOM) [51], providing a lighter softening of $M^{0\nu}$ with respect to the one provided by Jastrow type SRC.

It is useful to recall from Chapter 3 that the NME can be calculated as the sum of a Gamow-Teller (GT), a Fermi (F) and a Tensor (T) term.

$$M^{0\nu} = M_{GT}^{0\nu} - \left(\frac{g_V}{g_A}\right)^2 M_F^{0\nu} + M_T^{0\nu} \quad (5.4.6)$$

As the Tensor term is much smaller than the others it has been neglected in the present calculations.

Decay	Θ_{bare}	Θ_{eff}
$^{48}\text{Ca} \rightarrow ^{48}\text{Ti}$	0.53	0.30
$^{76}\text{Ge} \rightarrow ^{76}\text{Se}$	3.35	2.66
$^{82}\text{Se} \rightarrow ^{82}\text{Kr}$	3.30	2.72
$^{130}\text{Te} \rightarrow ^{130}\text{Xe}$	3.27	3.16
$^{136}\text{Xe} \rightarrow ^{136}\text{Ba}$	2.47	2.39

Table 4: $M^{0\nu}$ NME for the decays of all nuclei under examination. In the first column are reported the results obtained employing only the bare $0\nu\beta\beta$ -decay operator, in the second the ones with Θ_{eff} .

In Table 4, they are reported the calculated NME, and, for sake of completeness, they are also shown the results obtained when employing the bare $0\nu\beta\beta$ operator without any renormalization. As it can be seen, the effect of the renormalization of the operators is to reduce the value of $M^{0\nu}$. It is worth noting however, how this quenching is much smaller than the one obtained for the NME of $2\nu\beta\beta$.

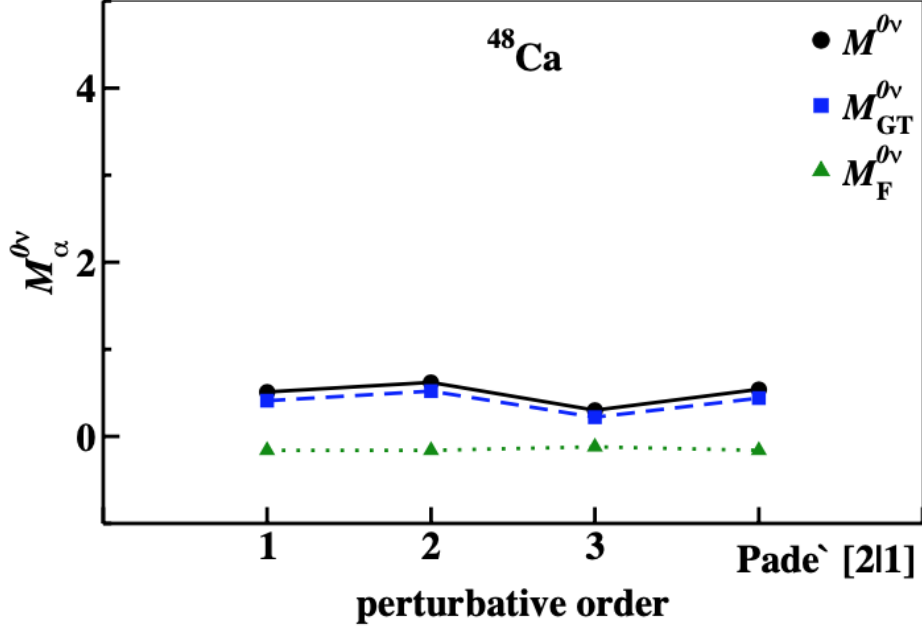


Figure 17: $M_\alpha^{0\nu}$ nuclear matrix elements for ^{48}Ca as a function of the perturbative order. Fig. taken from Ref. [55]

In Figures 17, 16 and 18 are shown, respectively, the values of $M^{0\nu}$, $M_{GT}^{0\nu}$ and $M_F^{0\nu}$ calculated for ^{48}Ca , ^{76}Ge , ^{82}Se , ^{130}Te , and ^{136}Xe from the bare operator up to effective operator at third order in perturbation theory. To further the effectiveness of this order-by-order comparisons and improve the perturbative behaviour of the results it is also shown the Padé approximant [2|1] of each of the different NME [56].

It is possible to observe that the perturbative behaviour of the $M^{0\nu}$ NMEs is dictated by the $M_{GT}^{0\nu}$ component and that the renormalisation procedure does not affect significantly the Fermi matrix element $M_F^{0\nu}$ for all the considered nuclei.

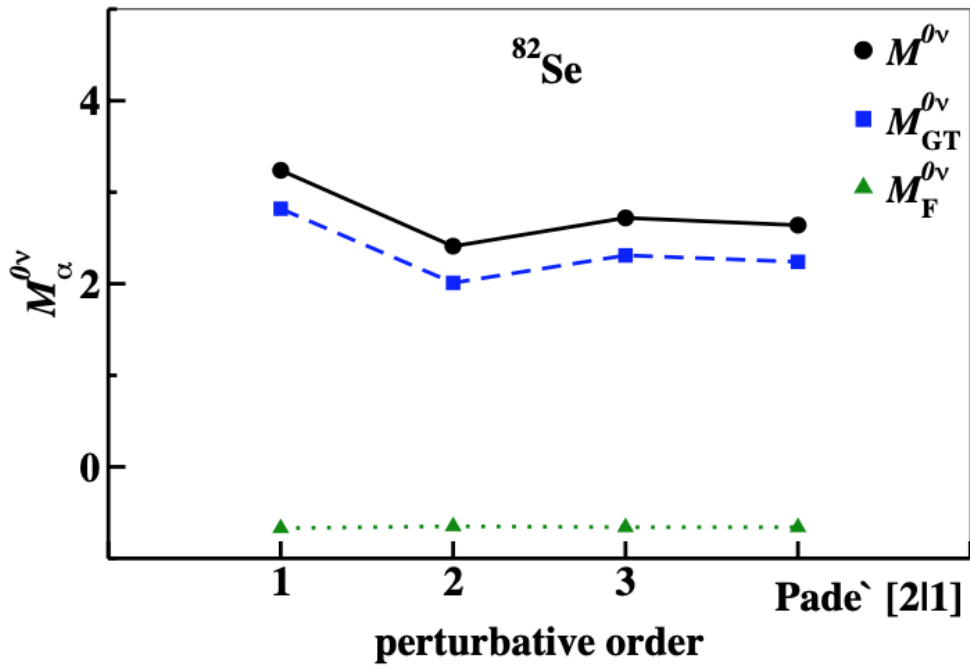
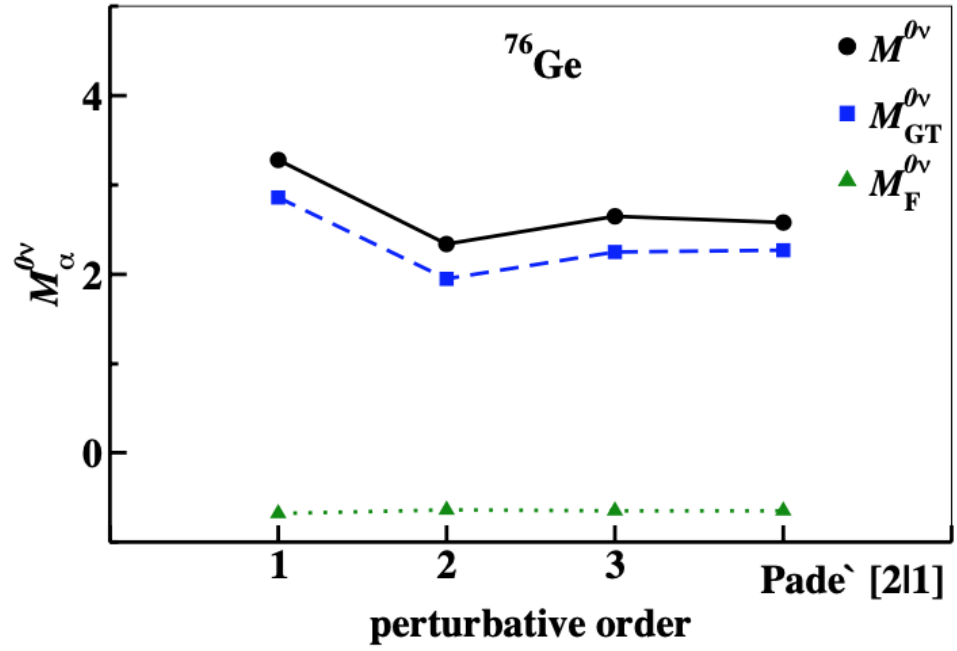


Figure 18: $M_\alpha^{0\nu}$ nuclear matrix element for ^{76}Ge and ^{82}Se as a function of the perturbative order. Fig. taken from Ref. [55]

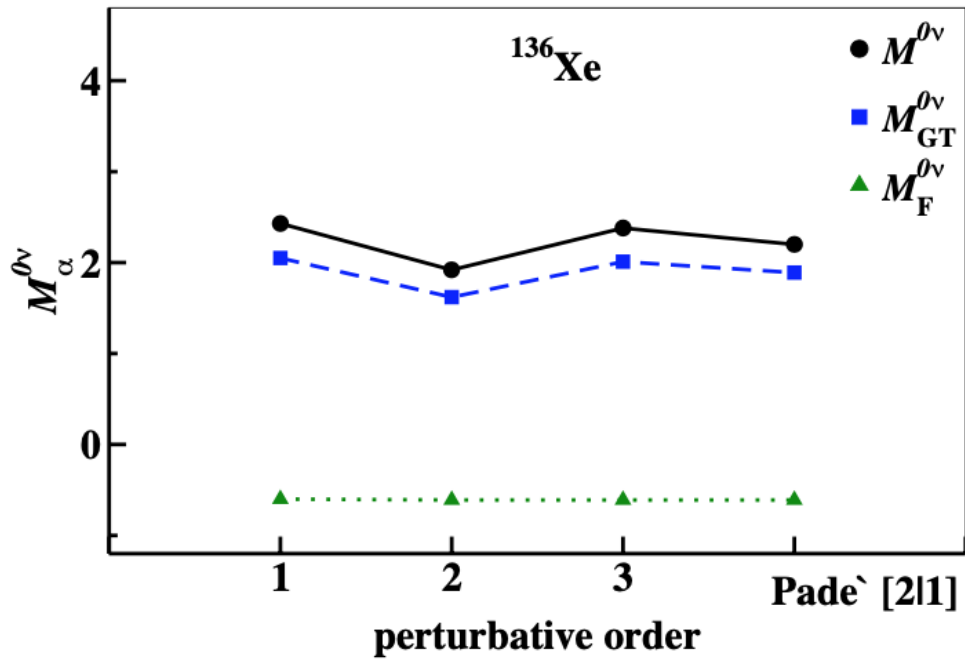
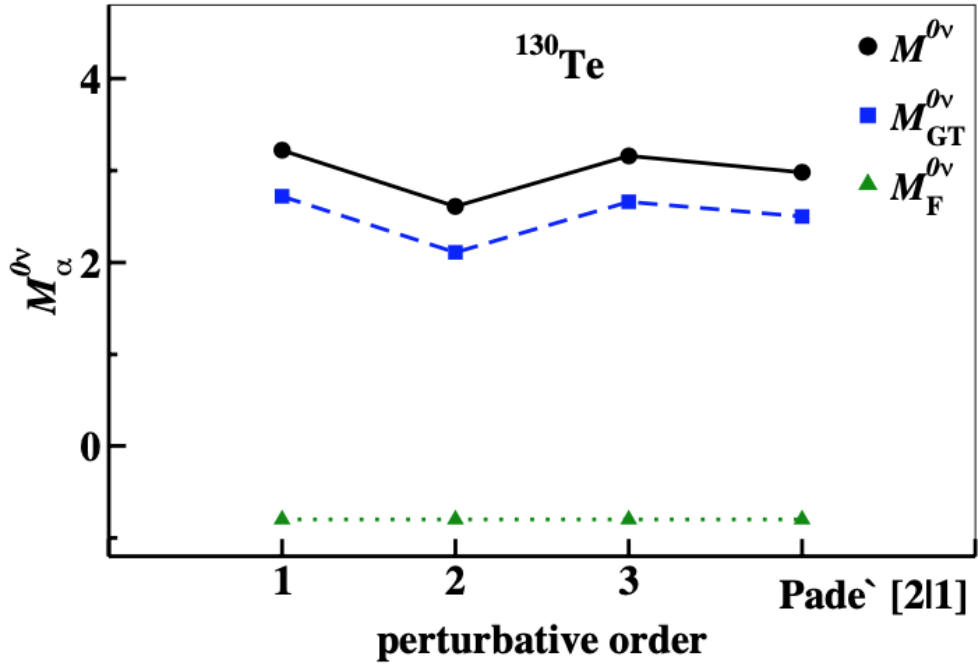


Figure 19: $M_{\alpha}^{0\nu}$ nuclear matrix elements for ^{130}Te and ^{136}Xe as a function of the perturbative order. Fig. taken from Ref. [55]

The difference between the second and third order results is much greater than that in the $2\nu\beta\beta$ and the convergence properties of the operator are less satisfactory. This does not come as a surprise as it was already established that the two operators have a different nature but this outcome deserves a more specific analysis.

Each of the previous partial NME $M_\alpha^{0\nu}$ can be then decomposed in terms of the total angular momentum and parity \mathcal{J}^π of the neutron-neutron couple of the initial state or, similarly, the proton-proton couple of the final state.

$$M_\alpha^{0\nu}(\mathcal{J}) = \sum_{j_p j_{p'} j_n j_{n'}} \langle j_p j_{p'}, \mathcal{J} | \tau_1^- \tau_2^- \Theta_\alpha | j_n j_{n'}, \mathcal{J} \rangle \langle f | a_p^\dagger a_{p'}^\dagger a_n a_{n'} | i \rangle \quad (5.4.7)$$

As it is apparent that the Gamow-Teller term yields the predominant contribution it is best to focus on it.

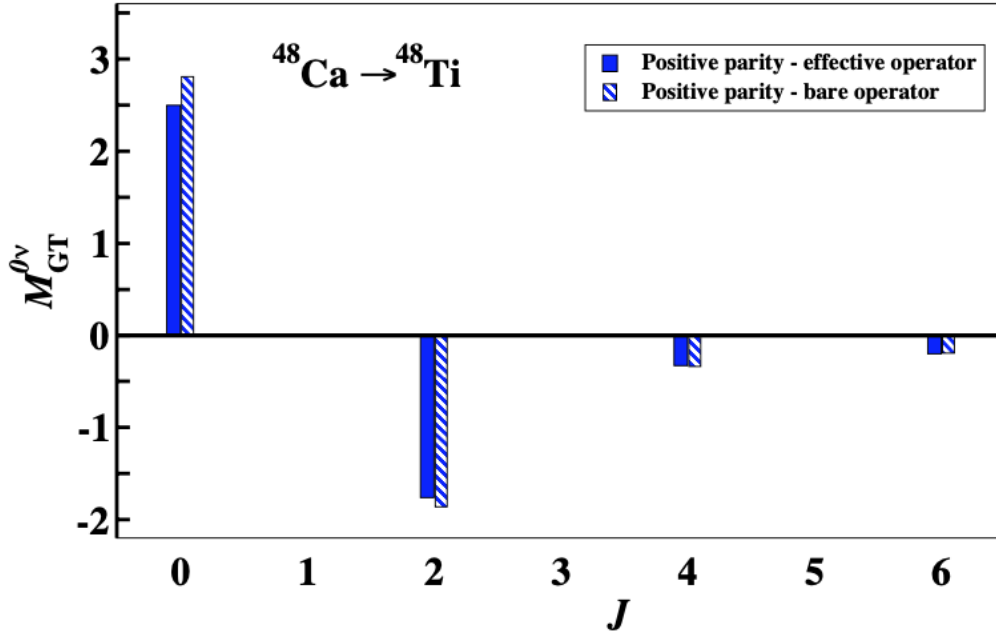


Figure 20: $M_{GT}^{0\nu}$ nuclear matrix element \mathcal{J} -pair decomposition and comparison between bare and third order operator for ^{48}Ca . Fig. taken from Ref. [55]

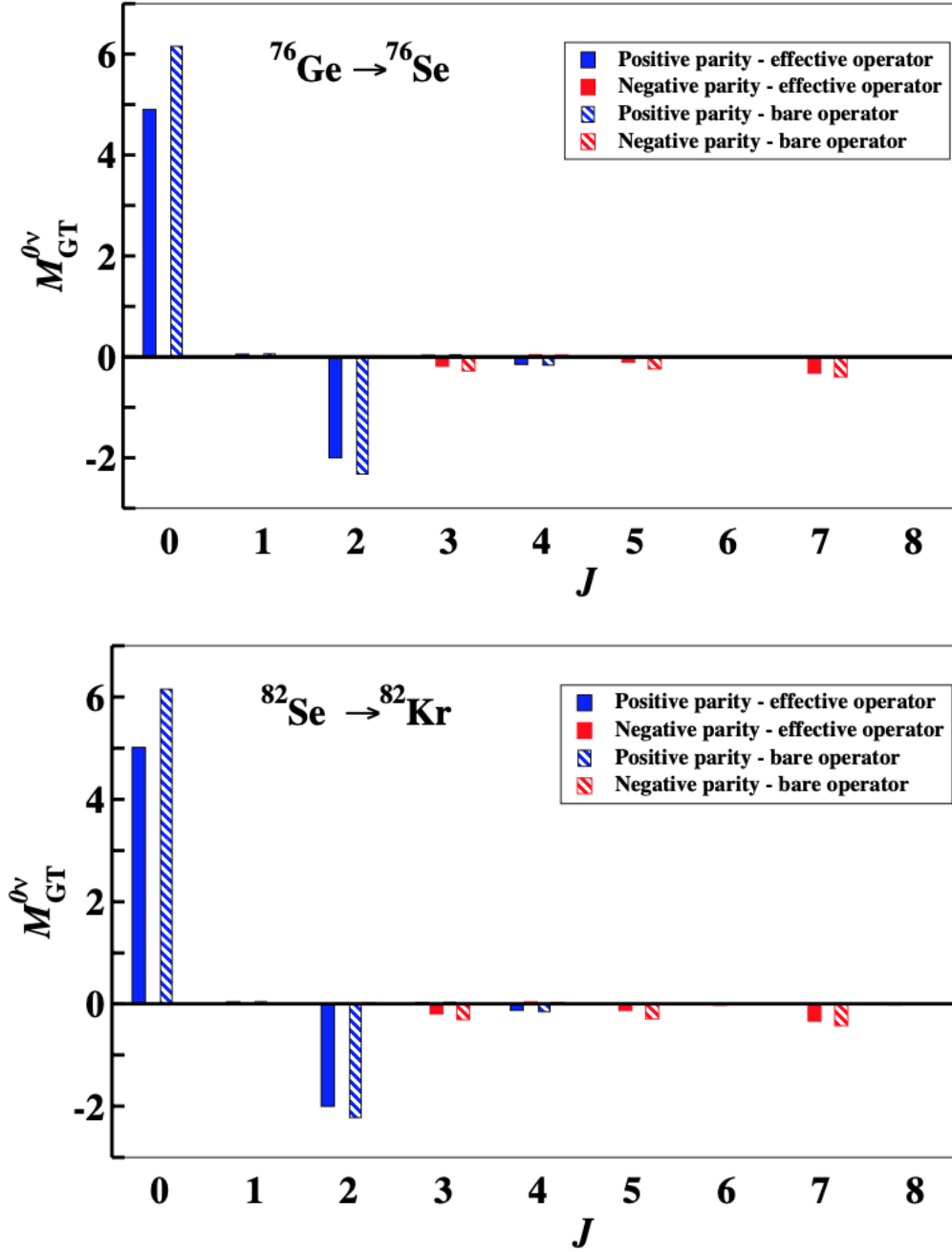


Figure 21: $M_{GT}^{0\nu}$ nuclear matrix element \mathcal{J} -pair decomposition and comparison between bare and third order operator for ^{76}Ge and ^{82}Se . Fig. taken from Ref. [55]

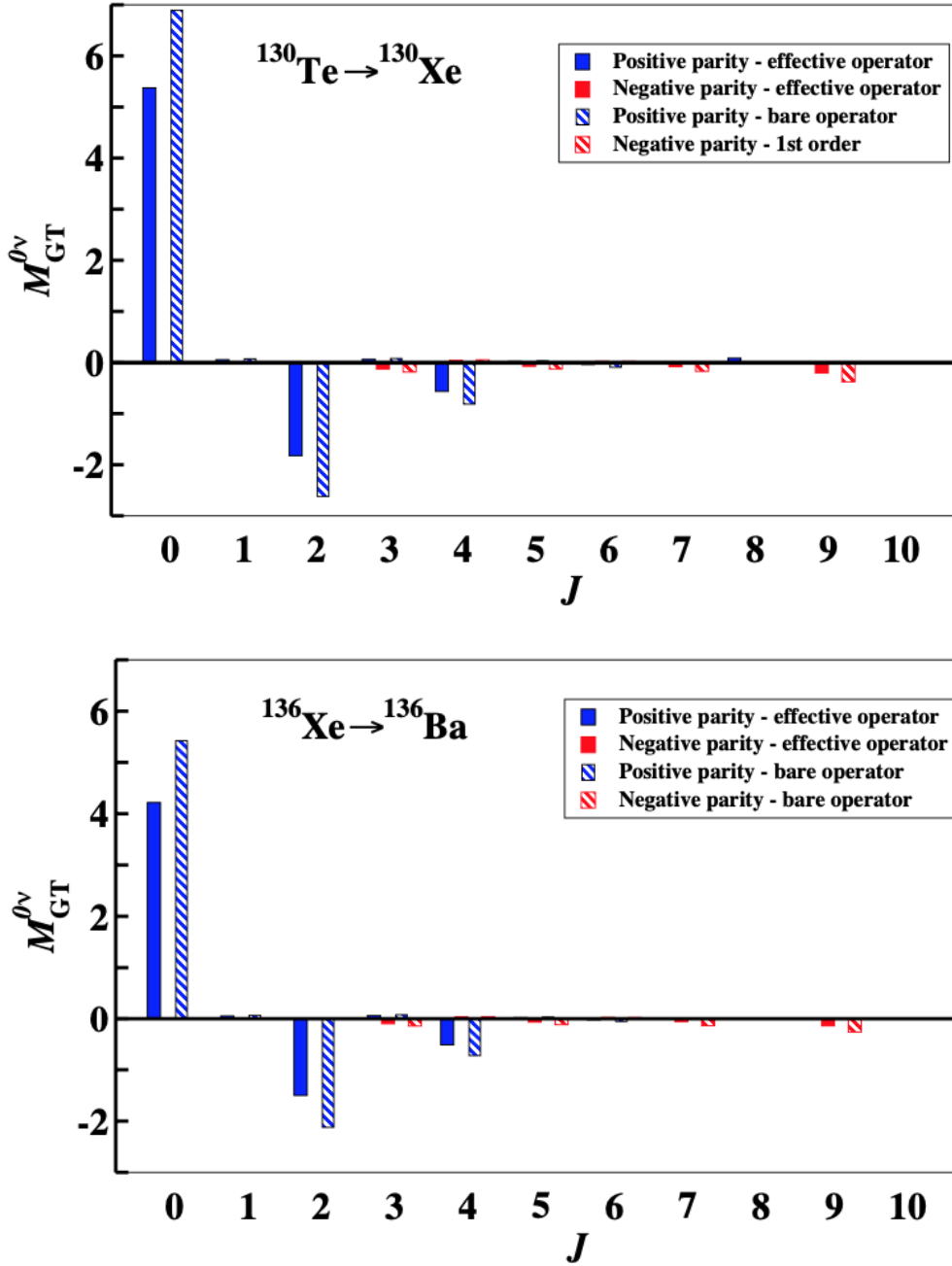


Figure 22: $M_{GT}^{0\nu}$ nuclear matrix element \mathcal{J} -pair decomposition and comparison between bare and third order operator for ^{130}Te and ^{136}Xe (in MeV^{-1}). Fig. taken from Ref. [55]

As is it possible to see from Fig. 20, 21 and 22 the main contributions to the NMEs are those corresponding to $\mathcal{J}^\pi = 0^+$ and $\mathcal{J} = 2^+$. For the heavier nuclei ^{130}Te and ^{136}Xe there is also a relative increase in the role played by the $\mathcal{J}^\pi = 4^+$ component.

In particular it is possible to observe a significant cancellation between the $\mathcal{J}^\pi = 0^+$ and the other contributions from states with even total angular momentum and positive parity $\mathcal{J}^\pi = 2n^+$. It is, also, remarkable that each J^π contribution to $M_{GT}^{0\nu}$ calculated employing the effective operator Θ_{eff} is smaller than the one obtained with the bare $0\nu\beta\beta$ -decay operator. This is to say that for each of the involved nuclei there is a quenching of each Gamow-Teller component in terms of the J^π decomposition.

For the sake of the completeness, it is worth noting that these results of the \mathcal{J}^π -decomposition are similar to those obtained in other SM calculations, as for example in Ref. [57, 17, 58, 59] for respectively the neutrinoless double-beta decay of ^{48}Ca , ^{76}Ge , ^{82}Se , ^{130}Te and ^{136}Xe .

5.5 Nuclear matrix elements for neutrinoless double-beta decay going beyond the closure approximation

In the following section are presented the RSM values of $M^{0\nu}$ calculated for ^{48}Ca and ^{136}Xe going beyond the closure approximation. These nuclei were chosen amongst the five candidate nuclei under exam because they are computationally easier to calculate.

The SM parameters are the same of the previous case when the closure approximation has been employed. The one-body transition densities ρ_{np} relative to the NMEs have been calculated with the KSHELL nuclear-shell model code [60, 61].

As already stated in Chapter 3 the beyond closure approach requires the use of non antisymmetrized two-body matrix elements. The current way of obtaining the effective operators is based on the use of antisymmetrized

vertices. For this reason, at least by now, the beyond closure method has been employed only to calculate the $0\nu\beta\beta$ nuclear matrix elements starting from the bare operators.

There are, however, no further theoretical obstacles and the general results obtained in this way can be extended without loss of generality to the case of the effective operators at higher order in perturbation theory.

Before proceeding further it is worth knowing as a first information how many intermediate states $|k, J_k\rangle$ are needed to reproduce the result obtained in closure approximation.

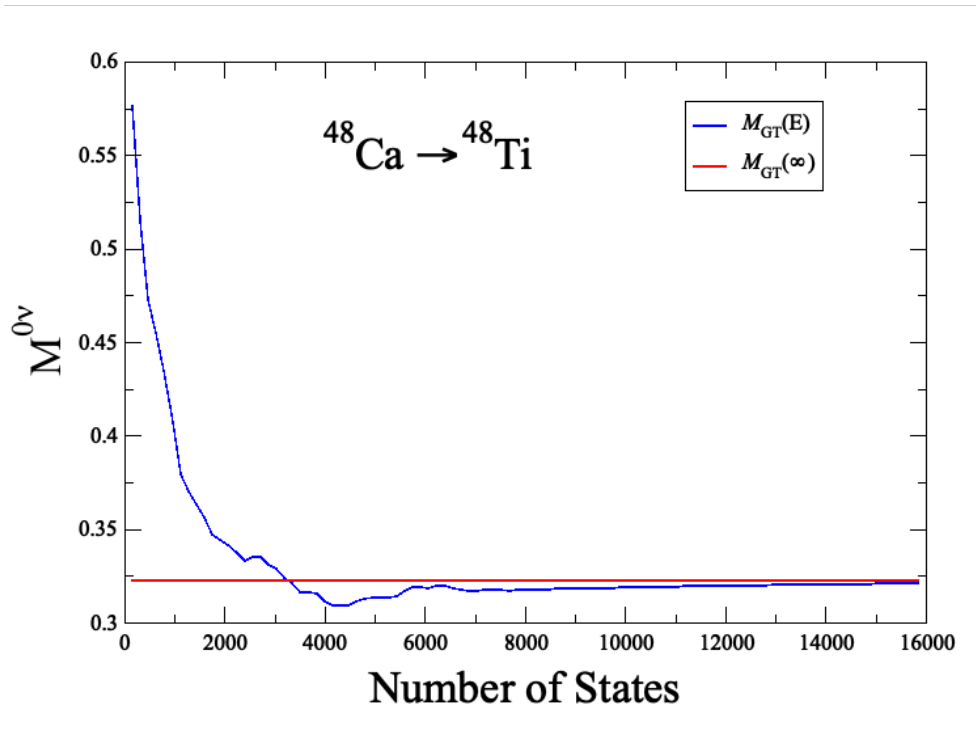


Figure 23: Convergence of the partial Gamow-Teller NME, $M_{GT}(E)$, for $0\nu\beta\beta$ decay of ^{48}Ca to its final value, $M_{GT}(\infty)$, obtained within closure approximation, as a function of the number of intermediate states.

The results for the case of ^{48}Ca are shown in Fig. 23. It is possible to see that 16000 intermediate states are needed corresponding to a maximum

excitation energy E_k of 22 MeV to reach convergence within 1% of the total result.

However, not all the intermediate states are needed to go beyond the closure approximation. At this point it is useful to recall from Eq. 3.4.4 the mixed NME $\bar{M}_\alpha^{0\nu}(\bar{E})$ given by the partial sum of all the intermediate states with $k < \bar{k}$ and a maximum excitation energy \bar{E} .

$$\bar{M}_\alpha^{0\nu}(\bar{E}) = M_\alpha^{0\nu}(\bar{E}) - \mathcal{M}_\alpha^{0\nu}(\bar{E}) + \mathcal{M}_\alpha^{0\nu}(\infty) \quad (5.5.1)$$

where $M_\alpha^{0\nu}(\bar{E})$ is the partial sum over of the all the intermediate states with $k < \bar{k}$ corresponding to an opportune cut-off to the excitation energy \bar{E} . That is to say that in the calculation of this NME the energy dependence of the energy value in the denominator of the neutrino potential has been preserved.

$\mathcal{M}_\alpha^{0\nu}(\bar{E})$, instead, is the NME calculated with the operators $\bar{\Theta}_\alpha$ where the energy dependence in the denominator of the neutrino potential has been replaced with an average value $\langle E \rangle$.

Finally $\mathcal{M}_\alpha^{0\nu}(\infty)$ is the result obtained within the closure approximation which was obtained in Section 4 of this Chapter. If one were to remove the cut-off to the excitation energy, i.e. for $\bar{E} \rightarrow \infty$, $\mathcal{M}_\alpha^{0\nu}(\bar{E})$ would converge to the result in closure approximation $\mathcal{M}_\alpha^{0\nu}(\infty)$. The difference between the closure and the non-closure approach when the excitation energy $E_k < \bar{E}$ is then equivalent to the difference $M_\alpha^{0\nu}(\bar{E}) - \mathcal{M}_\alpha^{0\nu}(\bar{E})$.

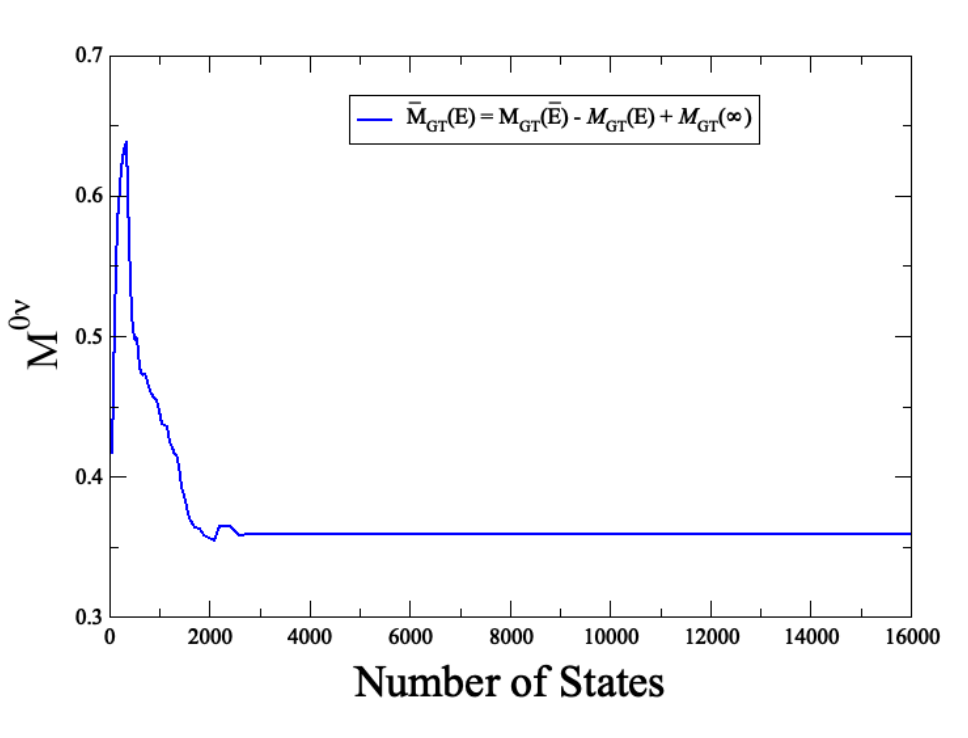


Figure 24: Convergence of the partial mixed Gamow-Teller NME, $\bar{M}_{GT}(E)$, for $0\nu\beta\beta$ decay of ^{48}Ca as a function of the number of intermediate states.

It is then possible to introduce a method which combines both the non-closure and closure approaches, by introducing the mixed NME $\bar{M}_\alpha^{0\nu}(\bar{E})$ that depends on the energy \bar{E} of the cut-off state \bar{k} . Since the main contribution to this difference comes from the Gamow-Teller term it is possible to specialise the previous assertions to the case $\alpha = \text{GT}$.

From Fig. 24 it is possible to observe that the behaviour of the convergence of the mixed MNE $\bar{M}_{GT}^{0\nu}(\bar{E})$ is much better than that of the simple partial sum $\mathcal{M}_{GT}^{0\nu}(\bar{E})$. Adopting the mixed method it is also possible to see that, in the case of ^{48}Ca the closure approximation affects the NME with a reduction of $\sim 11\%$ from $\bar{M}_{GT}^{0\nu}(\bar{E}) = 0.36$ to $\mathcal{M}_{GT}^{0\nu}(\infty) = 0.32$.

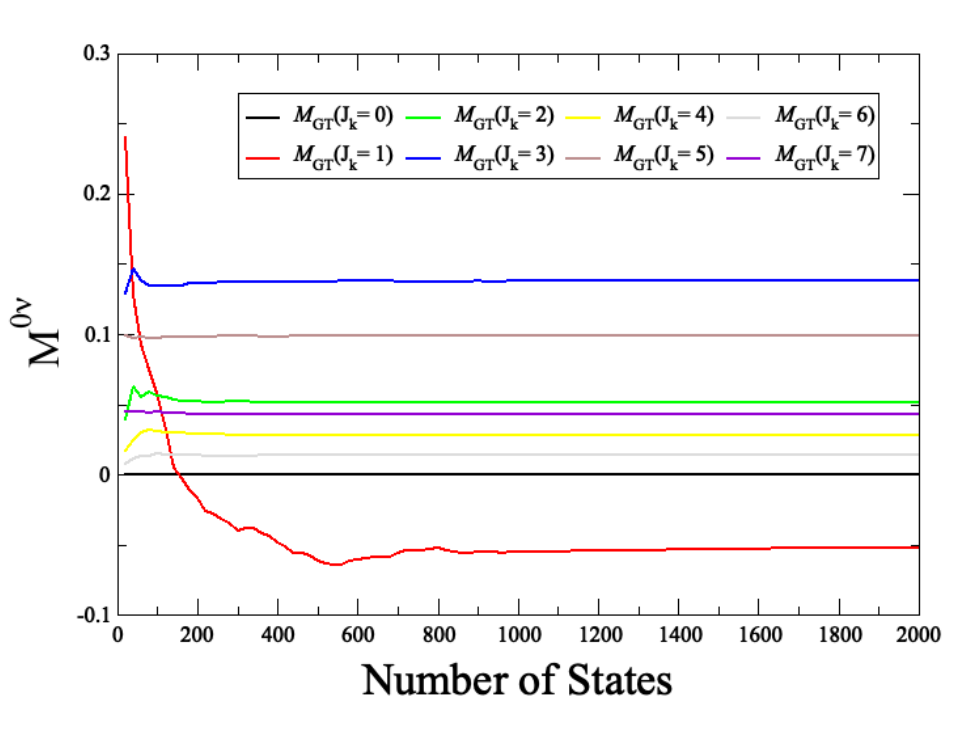


Figure 25: Convergence of the partial Gamow-Teller NME, $M_{GTk}(E)$, for $0\nu\beta\beta$ decay of ^{48}Ca as a function of the number of intermediate states

It is also useful to recall from Eq. 3.5.7 the expression for the partial NME $M_{\alpha k}^{0\nu}$ decomposed in term of the angular momentum and parity J_k^π of the intermediate state.

$$M_{\alpha k}^{0\nu} = \sum_{j_p j_{p'} j_n j_{n'}} \widehat{J}_k \widehat{J}_k \widehat{\mathcal{J}} (-1)^{j_n + j_{p'} + J_k + \mathcal{J}} \begin{Bmatrix} j_p & j_n & J_k \\ j_{n'} & j_{p'} & \mathcal{J} \end{Bmatrix} \quad (5.5.2)$$

$$\langle j_p j_{p'}, \mathcal{J} | \tau_1^- \tau_2^- \Theta_\alpha^k | j_n j_{n'}, \mathcal{J} \rangle \rho_{np}(J_k, i \rightarrow k) \rho_{n'p'}(J_k, k \rightarrow f)$$

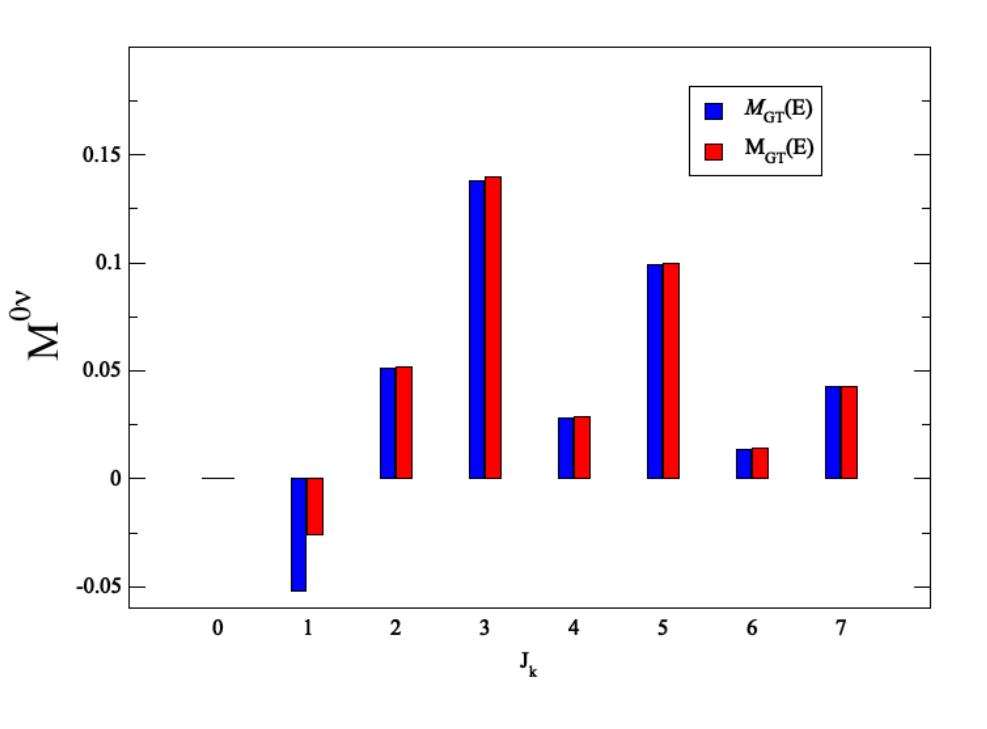


Figure 26: Comparison of the partial Gamow-Teller NME $M_{GT}^{0\nu}(E)$ and $\mathcal{M}_{GT}^{0\nu}(E)$ as a function of the total angular momentum of intermediate states J_k .

Since it is possible to decompose completely the problem in the angular momentum of the proton-neutron pair is also reasonable to imagine that the convergence of each component is different for different J_k . In fact it is apparent from a comparison between Fig. 23 and Fig. 25 that the convergence of the NME for ^{48}Ca is entirely determined by the states with $J_k = 1$.

From Fig. 26. it is also possible to see that the main difference between the partial NMEs obtained with the closure and non-closure approaches comes from contribution with intermediate angular momentum $J_k = 1$ and it is equal to $\sim 87\%$ of the total value of the $M_{GT}^{0\nu} - \mathcal{M}_{GT}^{0\nu}$ difference. The reason is that the $\sigma\tau_-$ operator naturally leads transitions from an initial 0^+ state to an intermediate 1^+ .

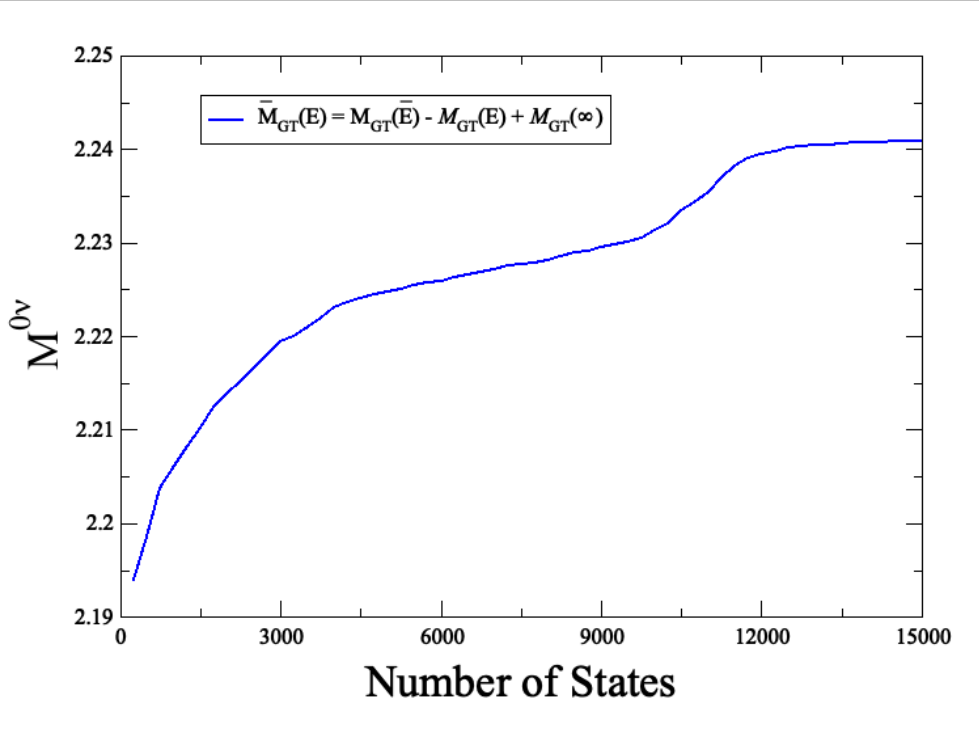


Figure 27: Convergence of the partial mixed Gamow-Teller NME, $\bar{M}_{GT}(E)$, for $0\nu\beta\beta$ decay of ^{136}Xe as a function of the number of intermediate states.

In the case of ^{136}Xe , contrary to that of ^{48}Ca , it was impossible to recover the convergence of the partial NMEs to the value obtained within the closure approximation. The first 15000 intermediate states, for a maximum excitation energy E_k of 8.1 MeV, were only able to account for $\sim 90\%$ of the final value. Nevertheless this number of intermediate states was sufficient to observe, as shown in Fig. 27, the convergence of the mixed MNE $\bar{M}_{GT}^{0\nu}(\bar{E})$.

It is also possible to see that the closure approximation is somewhat better suited for the $0\nu\beta\beta$ decay of ^{136}Xe than ^{48}Ca as the decrease of the NME is $\sim 7\%$, going from $\bar{M}_{GT}^{0\nu}(\bar{E}) = 2.24$ to $\mathcal{M}_{GT}^{0\nu}(\infty) = 2.09$.

To achieve the desirable accuracy significantly faster and with a lower number of intermediate states, contrary to the previous case of ^{48}Ca , the convergence of each partial NME $\bar{M}_{GTk}^{0\nu}$ has been evaluated singularly. As

it is possible to see from Fig. 28 the convergence of the partial NME for ^{136}Xe is mainly determined by the states with total angular momentum and parity $J_k^\pi = 1^+$, $J_k^\pi = 3^+$ and $J_k^\pi = 2^-$, for which more intermediate states are needed.

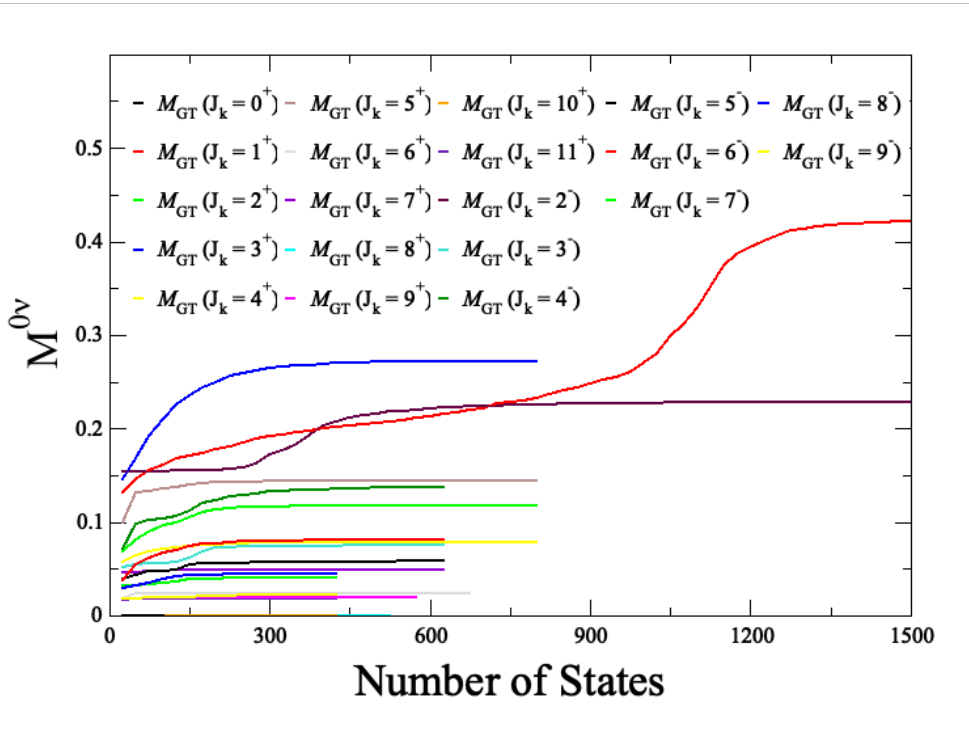


Figure 28: Convergence of the partial mixed Gamow-Teller NME, $\bar{M}_{GTk}(E)$, for $0\nu\beta\beta$ decay of ^{136}Xe as a function of the number of intermediate states.

A similar effect can be seen from the decomposition of the contribution to the difference between the two partial NMEs $M_{GT}^{0\nu}$ and $\mathcal{M}_{GT}^{0\nu}$. As it is shown in Fig. 29 the main contribution to difference between the partial NMEs $M_\alpha^{0\nu}(\bar{E}) - \mathcal{M}_\alpha^{0\nu}(\bar{E})$ comes from the already mentioned contribution from partial NMEs for $J_k^\pi = 1^+$, $J_k^\pi = 3^+$ and $J_k^\pi = 2^-$. The preponderance of these contribution is somewhat less pronounced than the case of ^{48}Ca , as they are responsible for $\sim 70\%$ of the difference $M_{GT}^{0\nu} - \mathcal{M}_{GT}^{0\nu}$. This result is in agreement with other studies conducted on ^{82}Se in Ref. [59] that identify the role of these contributions as the main source of the difference between

the closure approximation and the non-closure approach.

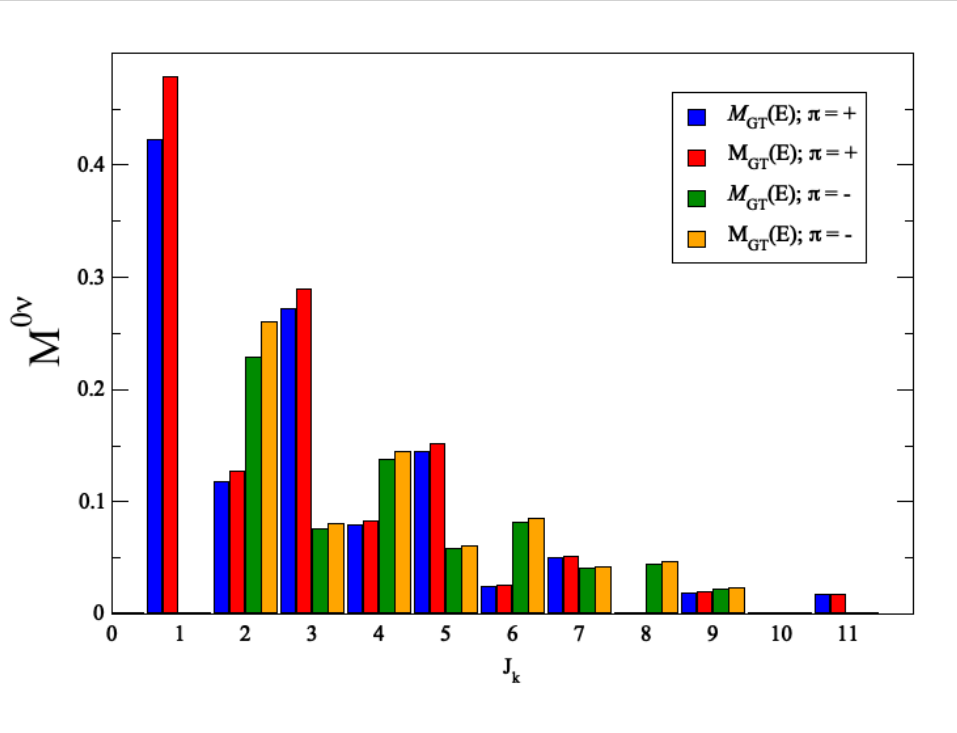


Figure 29: Comparison of the partial Gamow-Teller NME $M_{GT}^{0\nu}(E)$ and $\mathcal{M}_{GT}^{0\nu}(E)$ as a function of the total angular momentum of intermediate states J_k .

In the end by combining the non-closure and the closure approaches together it has been possible to estimate the uncertainty intrinsic in the closure approximation for the $0\nu\beta\beta$ NMEs of ^{48}Ca and ^{136}Xe . It is reasonable to assume that this effect also holds for other $0\nu\beta\beta$ -decay candidates as ^{78}Ge , ^{82}Se and ^{136}Xe . This mixed approach converges very quickly using only a very small number of states of the intermediate nucleus. Moreover the results obtained in this thesis work suggest that one can apply this mixed approach to obtain the shell-model $0\nu\beta\beta$ NMEs of decay of heavier nuclei focusing on the calculation only selected intermediate states with appropriate angular momentum and parity as $J_k^\pi = 1^+$, $J_k^\pi = 3^+$ and $J_k^\pi = 2^-$.

Chapter 6

Conclusions

The work of this thesis has been devoted to the calculation of the $0\nu\beta\beta$ NMEs for $^{48}\text{Ca} \rightarrow ^{48}\text{Ti}$, $^{76}\text{Ge} \rightarrow ^{76}\text{Se}$, $^{82}\text{Se} \rightarrow ^{82}\text{Kr}$, $^{130}\text{Te} \rightarrow ^{130}\text{Xe}$ and $^{136}\text{Xe} \rightarrow ^{136}\text{Ba}$ under the hypothesis of light-neutrino exchange.

The Realistic Shell Model [62, 55] has been used deriving consistently the shell-model effective Hamiltonians and operators. They have been obtained by way of many-body perturbation theory, starting from the realistic high-precision CD-Bonn NN potential [26] that has been renormalised to cure its non-perturbative behaviour caused by the repulsive high-momentum components, via the so-called $V_{\text{low-k}}$ approach [27]. This exactly preserves the on-shell properties of the original NN potential while also providing a smoother potential.

The foundation of this thesis lies in the work that has been done within the framework of the realistic shell model to calculate, by way of theoretical SM effective operators, the nuclear matrix elements $M^{2\nu}$ s for the $2\nu\beta\beta$ decays involving the same nuclei that are the object of this work [29]. These results have shown that, without resorting to empirical adjustments of H_{eff} , effective charges, gyromagnetic factors, or to the quenching of the axial coupling constant, the realistic shell model is able to provide a quantitative description of both spectroscopic properties (low-lying excitation spectra, electromagnetic transition strengths) and β decay (nuclear matrix elements of $2\nu\beta\beta$ decay, GT strengths from charge-exchange reactions).

Object of fundamental importance is the order-by-order perturbative behaviour of the effective two-body $0\nu\beta\beta$ -decay operator. While its convergence properties are not as satisfactory as the ones relative to the $2\nu\beta\beta$ -decay have been, this problem is far less important than the well-known one regarding the problem of the quenching of the axial vector current constant g_A [63, 36]. If one were to employ the quenching factor deduced by results for the $2\nu\beta\beta$ -decay to calculate the $M^{0\nu}$ NMEs the results would be much smaller than those shown in this thesis obtained with an effective $0\nu\beta\beta$ -decay operator.

It has also been possible to estimate the uncertainty intrinsic in the use of the closure approximation to calculate the $M^{0\nu}$ NMEs for ^{48}Ca and ^{136}Te . This has been done by highlighting the difference between the total matrix elements calculated within the closure approximation and those obtained when such approximation is not applied. To do so a mixed method has been developed. This difference is about 11% percent for the Gamow-Teller matrix element in the case of ^{48}Ca while for ^{136}Te the difference is about 8% percent. The difference between the results obtained with the two approaches for the Fermi term is negligible. While the beyond closure approach has been only applied to the bare operator the results can be extended to higher orders in perturbation theory.

In addition, it has also been possible to obtain a decomposition of the NMEs in terms of the total spin J_k of the intermediate states of the daughter nuclei. In the case of ^{48}Ca the $J_k = 1$ states provide the largest contribution to the difference between the closure and the beyond closure approach, while for the case of ^{136}Xe the states with $J_k = 1^+$, $J_k = 3^+$ and $J_k = 2^-$ all play an equally important role. It stands to reason that similar remarks should hold for the NMEs of other heavy nuclei that are candidate for $0\nu\beta\beta$ -decay, such as ^{76}Ge , ^{82}Se , ^{100}Mo and ^{130}Te .

The next step will be, as it has been mentioned in the previous Chapter, to extend the beyond closure approach to the effective neutrinoless double-beta decay operator even if this is a very demanding task in terms of computational resources. A possible further avenue to test the result obtained for the nuclear matrix elements is to perform a benchmark calculation of $M^{0\nu}$ for nuclei in the p-shell region and confront its results with those obtained with *ab initio* Quantum Monte Carlo calculations [64].

On another hand, it is worth investigating the renormalization of the $0\nu\beta\beta$ operator due to the subnucleonic degrees of freedom. To solve this issue one has to consistently derive an effective Hamiltonian and operators, starting from two- and three-body nuclear potentials derived within the framework of chiral perturbation theory [48, 65]. The contributions of chiral two-body electroweak currents must also be taken into account as some authors [66, 67] have found that β - and neutrinoless double-beta decays may be affected by these contributions.

List of Figures

1	Isobar for nuclei with $A=76$	7
2	Double β -decay diagrams	9
3	KamLAND-Zen effective Majorana neutrino mass $\langle m_{\beta\beta} \rangle$. . .	17
4	Energy shells of ^{18}O	28
5	Possible configurations for ^{18}O	29
6	Matrices H and H_{eff} for ^{18}O	30
7	$(V - U)$ -insertion diagram	40
8	Hard-core potential V_{NN} radial dependence	41
9	B(E2) transition probabilities: ^{48}Ca and ^{48}Ti	49
10	B(E2) transition probabilities: ^{76}Ge and ^{76}Se	49
11	B(E2) transition probabilities: ^{82}Se and ^{82}Kr	50
12	B(E2) transition probabilities: ^{130}Te and ^{130}Xe	50
13	B(E2) transition probabilities: ^{136}Xe and ^{136}Ba	51
14	$2\nu\beta\beta$ NME: Bare and Effective	53

15	$2\nu\beta\beta$ NME: Bare and Effective	55
16	$2\nu\beta\beta$ NME: Bare and Effective	56
17	$M_{\alpha}^{0\nu}$ NME : ^{48}Ca	60
18	$M_{\alpha}^{0\nu}$ NME : ^{76}Ge and ^{82}Se	61
19	$M_{\alpha}^{0\nu}$ NME: ^{130}Te and ^{136}Xe	62
20	$M_{GT}^{0\nu}$ \mathcal{J} -pair decomposition: ^{48}Ca	63
21	$M_{GT}^{0\nu}$ \mathcal{J} -pair decomposition: ^{76}Ge and ^{82}Se	64
22	$M_{GT}^{0\nu}$ \mathcal{J} -pair decomposition: ^{130}Te and ^{136}Xe	65
23	$\mathcal{M}_{GT}^{0\nu}$ convergence: ^{48}Ca	67
24	$\bar{M}_{GT}^{0\nu}$ convergence: ^{48}Ca	69
25	$\mathcal{M}_{GTk}^{0\nu}$ convergence: ^{48}Ca	70
26	Comparison between $M_{GT}^{0\nu}$ and $\mathcal{M}_{GT}^{0\nu}$: ^{48}Ca	71
27	$\bar{M}_{GT}^{0\nu}$ convergence: ^{136}Xe	72
28	$\bar{M}_{GTk}^{0\nu}$ convergence: ^{136}Xe	73
29	Comparison between $M_{GT}^{0\nu}$ and $\mathcal{M}_{GT}^{0\nu}$: ^{136}Xe	74

List of Tables

1	Half-life of the $2\nu\beta\beta$ decay	8
2	Neutrino oscillation parameters	12
3	$2\nu\beta\beta$ NME: Theoretical and Experimental	52
4	$M^{0\nu}$ NME summary table	59

Bibliography

- [1] B. Pontecorvo, “Inverse beta processes and nonconservation of lepton charge,” *Zh. Eksp. Teor. Fiz.*, vol. 34, p. 247, 1957.
- [2] V. N. Gribov and B. Pontecorvo, “Neutrino astronomy and lepton charge,” *Phys. Lett. B*, vol. 28, p. 493, 1969.
- [3] S. Bilenky and B. Pontecorvo, “Lepton mixing and neutrino oscillations,” *Physics Reports*, vol. 41, no. 4, pp. 225–261, 1978.
- [4] M. Goeppert-Mayer, “Double beta-disintegration,” *Phys. Rev.*, vol. 48, pp. 512–516, Sep 1935.
- [5] M. Tanabashi and *et al* *Phys. Rev. D*, vol. 98, p. 030001, Aug 2018.
- [6] E. Majorana, “Teoria simmetrica dell’elettrone e del positrone,” *Nuovo Cim.*, vol. 14, pp. 171–184, 1937.
- [7] W. H. Furry, “On transition probabilities in double beta-disintegration,” *Phys. Rev.*, vol. 56, pp. 1184–1193, Dec 1939.
- [8] K. A. Olive *et al.*, “Review of Particle Physics,” *Chin. Phys. C*, vol. 38, p. 090001, 2014.
- [9] J. Kotila and F. Iachello, “Phase-space factors for double- β decay,” *Phys. Rev. C*, vol. 85, p. 034316, Mar 2012.
- [10] J. Kotila and F. Iachello, “Phase space factors for $\beta^+\beta^+$ decay and competing modes of double- β decay,” *Phys. Rev. C*, vol. 87, p. 024313, Feb 2013.
- [11] J. Barea and F. Iachello *Phys. Rev. C*, vol. 79, p. 044301, Apr 2009.

- [12] J. Barea, J. Kotila, and F. Iachello *Phys. Rev. Lett.*, vol. 109, p. 042501, Jul 2012.
- [13] J. Barea, J. Kotila, and F. Iachello *Phys. Rev. C*, vol. 87, p. 014315, Jan 2013.
- [14] A. Gando, Y. Gando, T. Hachiya, A. Hayashi, S. Hayashida, H. Ikeda, K. Inoue, K. Ishidoshiro, Y. Karino, M. Koga, S. Matsuda, T. Mitsui, K. Nakamura, S. Obara, T. Oura, H. Ozaki, I. Shimizu, Y. Shirahata, J. Shirai, A. Suzuki, T. Takai, K. Tamae, Y. Teraoka, K. Ueshima, H. Watanabe, A. Kozlov, Y. Takemoto, S. Yoshida, K. Fushimi, T. I. Banks, B. E. Berger, B. K. Fujikawa, T. O'Donnell, L. A. Winslow, Y. Efremenko, H. J. Karwowski, D. M. Markoff, W. Tornow, J. A. Detwiler, S. Enomoto, and M. P. Decowski, "Search for majorana neutrinos near the inverted mass hierarchy region with kamland-zen," *Phys. Rev. Lett.*, vol. 117, p. 082503, Aug 2016.
- [15] W. C. Haxton and G. J. Stephenson Jr. *Prog. Part. Nucl. Phys.*, vol. 12, p. 409, 1984.
- [16] T. Tomoda *Rep. Prog. Phys.*, vol. 54, p. 53, 1991.
- [17] R. A. Sen'kov and M. Horoi *Phys. Rev. C*, vol. 88, p. 064312, Dec 2013.
- [18] K. Suzuki and S. Y. Lee *Prog. Theor. Phys.*, vol. 64, p. 2091, 1980.
- [19] T. H. Schucan and H. A. Weidenmüller *Ann. Phys. (N.Y.)*, vol. 73, p. 108, 1972.
- [20] T. H. Schucan and H. A. Weidenmüller *Ann. Phys. (N.Y.)*, vol. 76, p. 483, 1973.
- [21] E. M. Krenciglowa and T. T. S. Kuo *Nucl. Phys. A*, vol. 235, p. 171, 1974.
- [22] T. T. S. Kuo, F. Krmpotić, K. Suzuki, and R. Okamoto *Nucl. Phys. A*, vol. 582, p. 205, 1995.
- [23] K. Suzuki and R. Okamoto *Prog. Theor. Phys.*, vol. 70, p. 439, 1983.
- [24] H. A. Bethe *Annu. Rev. Nucl. Sci.*, vol. 21, p. 93, 1971.

- [25] K. Suzuki and R. Okamoto *Prog. Theor. Phys.*, vol. 93, p. 905, 1995.
- [26] R. Machleidt *Phys. Rev. C*, vol. 63, p. 024001, 2001.
- [27] S. Bogner, T. T. S. Kuo, L. Coraggio, A. Covello, and N. Itaco *Phys. Rev. C*, vol. 65, p. 051301(R), 2002.
- [28] L. Coraggio, A. Gargano, and N. Itaco, “Role of three-nucleon forces in neutron-rich nuclei beyond ^{132}Sn ,” *JPS Conf. Proc.*, vol. 6, p. 020046, 2015.
- [29] L. Coraggio, L. De Angelis, T. Fukui, A. Gargano, N. Itaco, and F. Nowacki *Phys. Rev. C*, vol. 100, p. 014316, Jul 2019.
- [30] Data extracted using the NNDC On-line Data Service from the ENSDF database, file revised as of March 15, 2019.
- [31] Data extracted using the NNDC On-line Data Service from the XUNDL database, file revised as of March 15, 2019.
- [32] A. Barabash, “Precise half-life values for two-neutrino double- decay: 2020 review,” *Universe*, vol. 6, no. 10, 2020.
- [33] E. Caurier, G. Martínez-Pinedo, F. Nowacki, A. Poves, and A. P. Zuker *Rev. Mod. Phys.*, vol. 77, pp. 427–488, Jun 2005.
- [34] E. Caurier and F. Nowacki *Acta Phys. Pol. B*, vol. 30, p. 705, 1999.
- [35] E. Caurier, G. Martínez-Pinedo, F. Nowacki, A. Poves, and A. P. Zuker, “The shell model as a unified view of nuclear structure,” *Rev. Mod. Phys.*, vol. 77, pp. 427–488, Jun 2005.
- [36] J. T. Suhonen *Frontiers in Physics*, vol. 5, p. 55, 2017.
- [37] T. S. Park, D. P. Min, and M. Rho *Phys. Rep.*, vol. 233, p. 341, 1993.
- [38] S. Pastore, L. Girlanda, R. Schiavilla, M. Viviani, and R. B. Wiringa *Phys. Rev. C*, vol. 80, p. 034004, Sep 2009.
- [39] M. Piarulli, L. Girlanda, L. E. Marcucci, S. Pastore, R. Schiavilla, and M. Viviani *Phys. Rev. C*, vol. 87, p. 014006, Jan 2013.

- [40] A. Baroni, L. Girlanda, S. Pastore, R. Schiavilla, and M. Viviani *Phys. Rev. C*, vol. 93, p. 015501, Jan 2016.
- [41] J. Blomqvist and A. Molinari *Nucl. Phys. A*, vol. 106, p. 545, 1968.
- [42] L. Coraggio, A. Covello, A. Gargano, and N. Itaco, “Shell-model calculations for neutron-rich carbon isotopes with a chiral nucleon-nucleon potential,” *Phys. Rev. C*, vol. 81, p. 064303, Jun 2010.
- [43] L. Coraggio, A. Covello, A. Gargano, N. Itaco, and T. T. S. Kuo *Ann. Phys. (NY)*, vol. 327, p. 2125, 2012.
- [44] L. Coraggio, L. De Angelis, T. Fukui, A. Gargano, and N. Itaco, “Two-neutrino double-beta decay within the realistic shell model,” *J. Phys. Conf. Ser.*, vol. 1056, p. 012012, 2018.
- [45] P. J. Ellis and E. Osnes *Rev. Mod. Phys.*, vol. 49, p. 777, 1977.
- [46] E. Caurier, F. Nowacki, and A. Poves *Eur. Phys. J. A*, vol. 15, pp. 145–150, 2002.
- [47] N. Itaco, L. Coraggio, and R. Mancino *Eur. Phys. J. Web of Conferences*, vol. 223, p. 01025, 2019.
- [48] Y. Z. Ma, L. Coraggio, L. De Angelis, T. Fukui, A. Gargano, N. Itaco, and F. R. Xu, “Contribution of chiral three-body forces to the monopole component of the effective shell-model hamiltonian,” *Phys. Rev. C*, vol. 100, p. 034324, Sep 2019.
- [49] G. A. Miller and J. E. Spencer *Ann. Phys. (NY)*, vol. 100, p. 562, 1976.
- [50] A. Neacsu, S. Stoica, and M. Horoi *Phys. Rev. C*, vol. 86, p. 067304, Dec 2012.
- [51] J. Menéndez, A. Poves, E. Caurier, and F. Nowacki *Nucl. Phys. A*, vol. 818, p. 139, 2009.
- [52] M. Kortelainen, O. Civitarese, J. Suhonen, and J. Toivanen *Phys. Lett. B*, vol. 647, p. 128, 2007.
- [53] H. Feldmeier, T. Neff, R. Roth, and J. Schnack *Nucl. Phys. A*, vol. 632, p. 61, 1998.

- [54] F. Andreozzi *Phys. Rev. C*, vol. 54, p. 684, 1996.
- [55] L. Coraggio, A. Gargano, N. Itaco, R. Mancino, and F. Nowacki *Phys. Rev. C*, vol. 101, p. 044315, Apr 2020.
- [56] G. A. Baker and J. L. Gammel, *The Padé Approximant in Theoretical Physics*, vol. 71 of *Mathematics in Science and Engineering*. Academic Press, New York, 1970.
- [57] C. F. Jiao, M. Horoi, and A. Neacsu *Phys. Rev. C*, vol. 98, p. 064324, Dec 2018.
- [58] R. A. Sen'kov and M. Horoi *Phys. Rev. C*, vol. 93, p. 044334, Apr 2016.
- [59] R. A. Sen'kov, M. Horoi, and B. A. Brown *Phys. Rev. C*, vol. 89, p. 054304, May 2014.
- [60] N. Shimizu, “Nuclear shell-model code for massive parallel computation, ”kshell”,” 2013.
- [61] N. Shimizu, T. Mizusaki, Y. Utsuno, and Y. Tsunoda, “Thick-restart block lanczos method for large-scale shell-model calculations,” *Computer Physics Communications*, vol. 244, pp. 372–384, 2019.
- [62] L. Coraggio, A. Covello, A. Gargano, N. Itaco, and T. T. S. Kuo *Prog. Part. Nucl. Phys.*, vol. 62, p. 135, 2009.
- [63] J. Suhonen *Phys. Rev. C*, vol. 96, p. 055501, Nov 2017.
- [64] G. B. King, L. Andreoli, S. Pastore, and M. Piarulli, “Weak transitions in light nuclei,” *Frontiers in Physics*, vol. 8, p. 363, 2020.
- [65] T. Fukui, L. De Angelis, Y. Z. Ma, L. Coraggio, A. Gargano, N. Itaco, and F. R. Xu, “Realistic shell-model calculations for p -shell nuclei including contributions of a chiral three-body force,” *Phys. Rev. C*, vol. 98, p. 044305, Oct 2018.
- [66] L.-J. Wang, J. Engel, and J. M. Yao, “Quenching of nuclear matrix elements for $0\nu\beta\beta$ decay by chiral two-body currents,” *Phys. Rev. C*, vol. 98, p. 031301, Sep 2018.

- [67] P. Gysbers, G. Hagen, J. D. Holt, G. R. Jansen, T. D. Morris, P. Navrátil, T. Papenbrock, S. Quaglioni, A. Schwenk, S. R. Stroberg, and K. A. Wendt *Nature Phys.*, vol. 15, p. 428, 2019.